Student thesis series INES nr 405

Porous asphalt as a method for reducing urban storm water runoff in Lund, Sweden

Gea Hallen

2016

Department of

Physical Geography and Ecosystem Science

Lund University

Sölvegatan 12

Gea Hallen (2016) **Porous asphalt as a method for reducing urban storm water runoff in Lund, Sweden**

Master degree thesis, 30 credits in Geomatics

Department of Physical Geography and Ecosystem Science, Lund University

Level: Master of Science (MSc)

Course duration: *January* 2014 until *June* 2016

Disclaimer

This document describes work undertaken as part of a program of study at the University of Lund. All views and opinions expressed herein remain the sole responsibility of the author, and do not necessarily represent those of the institute.

Porous asphalt as a method for reducing urban storm water runoff in Lund, Sweden

---

Gea Hallen

Master thesis, 30 credits, in Geomatics

Supervisor: Andreas Persson

Senior lecturer at Dept. of Physical Geography and Ecosystems Science

Exam committee:

Examiner 1: Ulrik Mårtensson

Director of studies at Dept. of Physical Geography and Ecosystems Science

Examiner 2: Abdulghani Hasan

Senior lecturer at Dept. of Physical Geography and Ecosystems Science

Abstract

The risk of urban flooding has grown as a result of fast urbanization. Changing pervious surfaces to impervious ones has caused the increase in surface runoff that causes overflowing from the existing drainage systems. A new approach for mitigating flood hazard in the form of Low Impact Development (LID) has emerged to reverse the negative impacts of the built up areas. As one of numerous practices, porous asphalt is used to model the runoff reduction potential for a residential neighborhood in Lund, Sweden. The modelling is undertaken using Storm Water Management Model (SWMM) with simulations results for 'No Change' scenarios compared with results after the implementation of porous asphalt pavement. Site location selection for the LID practice is based on the flow accumulation streams and highest flooded inlets. Modelling results confirm the effectiveness of porous asphalt in reducing flooded water volumes by 65.6%, 77.5% and 99.2% during 100, 50 and 10 year return rainfall evens respectively. Water volumes classified as flooding do not significantly reduce as storage capacity gets increased from 0.25 meters to 0.5 meters.

Key words: PCSWMM, urban flood modelling, porous asphalt

Acknowledgements

First, I would like to thank my supervisor, Andreas Persson for his continuous support and encouragement throughout the thesis writing period. Secondly, the study could not have been carried out without the generous gesture by Bill James, offering the license for PCSWMM for the research. Additionally, I would like to express my gratitude to the following people: Rolf Larsson for helping me to obtain the modelling license; Mark Randall for guiding me with the running of the model; Lemiss Sebty, Thomas Åkerholm, Johanna Sörensen, Shuzhi Dong and Abdalla Eltayeb for their help in collecting the necessary data.

Table of Contents

List of Figures

List of Tables

List of Abbreviations

DEM	Digital Elevation Model
EPA	Environmental Protection Agency
GI	Green Infrastructure
GIS	Geographical Information Systems
GPS	Global Positioning System
LID	Low Impact Development
SWMM	Storm Water Management Model

1. Introduction

Urban floods have become an increasing risk for the ever growing residents of metropolitan areas. The UNISDR (United Nations Office for Disaster Risk Reduction) has reported that for 616 major metropolitan areas river floods are by far the most damaging natural hazard, threatening over 379 million urban residents, with earthquake and strong winds potentially affecting 283 million and 157 million, respectively. Rapid urbanization trend is expected to continue with estimations of already 66 per cent of the world's population projected to be living in urban areas by 2050 (Lewis and Purcell, 2014).

The natural causes for urban flooding are usually the result of a combination of meteorological and hydrological extremes, such as high precipitation and flows. On the other hand, floods have also resulted due to human activities, such as growth of unplanned settlements, development on floodplains, breach of dams or failed embankment (Jha et al, 2012). For both cases there are usually two underlying factors that increase the flood risk in an urban environment even more: the land use change and the failure of the drainage systems. The first factor is caused by the compacting of pervious soils due to the high concentration of buildings and the covering of the areas with impervious surfaces such as roofs and asphalt pavements. Impervious surfaces however have a negative impact on the natural hydrological cycle of the area. Changing areas from pervious to impervious prevents the infiltration of surface water into the ground, increasing greatly storm runoffs in terms of volumes and peak flow and consequently causing floods in cities (Liu et al., 2014).

The second factor is the overloaded drainage system, which fail to remove excess water during intense rainfall events and cause overflow from the inlets back to the surface. The drainage system varies significantly across countries from being almost non-existent to having the storm water drainage combined or separate from the sewage network. In countries, such as Sweden, larger cities started to build wastewater systems in the late 1880s with combined sewer systems being the preferred type (Swedish EPA, 2014). A combined sewer system (CSS) collects all waste together into the same pipe: rainwater runoff, domestic sewage and industrial wastewater (Geels, 2006). However, with the growth of population and especially during high precipitation events the capacity of the designed drainage systems is exceeded causing water spillage from manholes, basement inundations and increased surface runoff

(Niea et al., 2009). This is especially problematic in the older parts of the cities where the combined sewer system has not been replaced with a separate one which would lessen the volume in the pipes and treatment plans by discharging the rainwater flow directly to a local receiving water (Butler and Davis, 2004).

To reduce the urban flood hazard that besides the significant risk to human life also results in traffic interruptions, economic losses, pollution and health issues (Yao et al., 2016) a new approach has risen in recent years in the form of implementation of Green Infrastructure (GI). GI installations consist of systems and practices that utilize or mimic the natural processes, allowing storm water to infiltrate, evaporate, runoff, and/or be used on-site (Liu et al. 2014). One of the many options for such infrastructure is permeable pavement that contrary to regular impervious pavements allows storm water to penetrate much faster into an underlying storage base and subsequently release it to the subgrade or sewer network. This study focuses on one type of permeable pavement option, porous asphalt. Porous asphalt designs themselves vary greatly as well, but the general idea behind the mixtures involves an open-graded aggregate layer that increases the size of permeable air voids allowing water to penetrate through the voids and removing it from the surface (Putman and Kline, 2012).

1.1 Objectives

The study applies PCSWMM *(detailed explanation in Section 3.3)* modelling to a section of Lund that has experienced flooding during heavy rainfall events in the recent past. The study proposes that through the implementation of porous asphalt flooding volume and intensity could be reduced significantly. Firstly, the goal is to identify the areas with the highest risk of drainage inlet overflow using simulated rainfall with low to severe intensities. Secondly, sections of currently impenetrable surfaces will be chosen for the implementation of porous asphalt. Thereafter, the model will be run again using the modified pavement data with the same simulated rainfall. Comparisons will be made concerning the change in flooded volumes before and after the implementation of porous asphalt in the model. In addition, the capacity of different porous asphalt designs in coping with the varying rainfall intensities will be analyzed.

The study aims to answer the following questions:

1. What is the capacity of porous asphalt in reducing runoff volume during 1, 10, 50 and 100 year return rainfall events?
2. What is the optimal design (e.g. stone reservoir capacity) of the porous asphalt for the study area?
3. How effective is PCSWMM in simulating accumulating flood risk for the whole study area?

There are many green infrastructure methods that could potentially reduce the flood problem for the proposed study area. This study focuses on porous asphalt as one of those options.

1.2 The study area

The study area is located in the northern part of Lund (Figure 1). It is a suburban area covering approximately 0.14 km^2, served with a separate storm water system from the sewer network. The area was selected based on suggestions from the regional sewer treatment and drinking water providing company VA Syd who had recorded continuous flooding problems (e.g. in 2000 and 2009) in that neighborhood. In communication with the company it was understood that the previously recorded flooding events south of the study area had mainly been caused by the excess storm water running off from Gästgivarevägen street (and the surrounding streets of Nyckelkroken, Gilleskroken, Vapenkroken and Källarekroken). The area is rather flat with an average slope directed towards the south-west. The area consists of typically private houses with surrounding gardens separated by paved roads. Approximately 52% of the study area is under pervious land cover (grass, trees) and 48% built-up (streets, roofs). The area around Gästgivarevägen street, 25 meters from either side, is aligned with wide paved car parking lots and has therefore and average imperviousness percentage of 80.5%. The existing drainage system was designed to gather the runoff water from the area and directing it west towards Vittnesgränden street, however during strong rain events the drainage system gets overloaded and the surplus water flows south following the natural topography and causing flooding south of the study area.

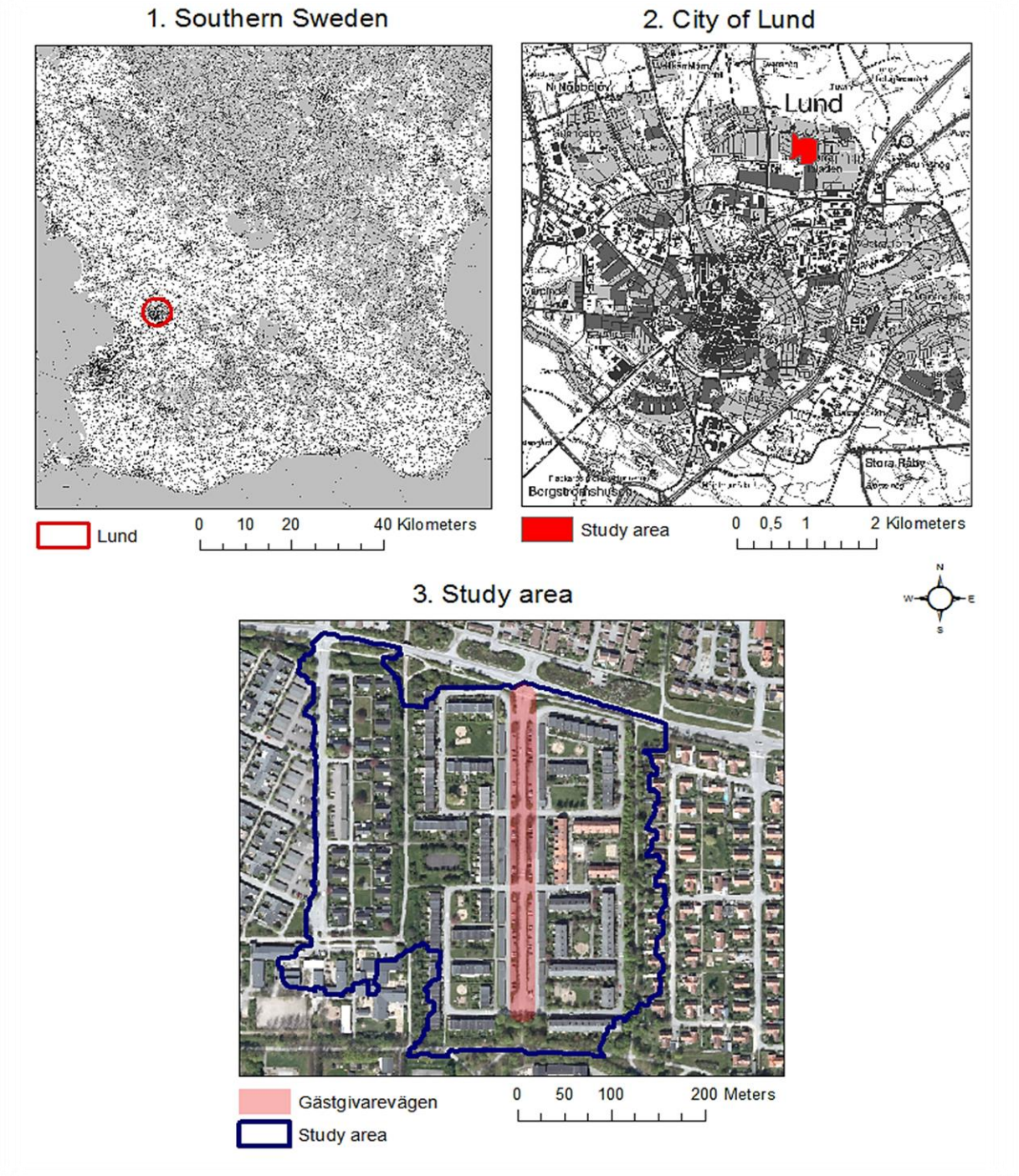

Figure 1. The Study area.

The Study area is located in the northern part of Lund, Sweden. Image 1 shows the location of the city of Lund located in the southern part of Sweden. Image 2 shows the location of the study area in the northern part of the city. Image 3 illustrates the delineated study area and highlights the Gästgivarevägen street.

2 Theoretical background

2.1 Hydrological modeling

Increasing number of storm water flow models together with Geographical Information Systems (GIS) have become very popular in evaluating the storm-readiness and climate resilience of cities and analyzing the effects of various storm water management strategies (Jain et al. 2016). This has been coupled with the rise of accessible data, especially thanks to the increase of the quality of remotely sensed data. The availability of sub-meter resolution satellite images and very high-resolution digital elevation models (DEMs) allow better estimation of the required parameters and therefore more accurate rainfall-runoff simulations in areas with complex landscapes, such as the urban environments (Jain et al. 2016).

High quality data is especially important for estimating parameter values for physically based distributed hydrological models. Physically based models calculate the water balance of the hydrological cycle by taking into account processes, such as infiltration, evapotranspiration, flow aggregation, groundwater recharge, etc. and using parameters that could be directly measured from the real world (Kunstmann et al., 2006). Contrary to lumped models that treat the catchment as a single unit with assigned parameters representing the averages over the whole area, physically based (also referred to as distributed) models divide the larger subcatchment into smaller units and make predictions based on local parameters (Beven, 2012). SWMM, a semi-distributed model assigns these variables for each user defined parcel with characteristics for a number of variables such as infiltration, slope, depression storage, etc. These variables, although high in numbers, can be calculated in combination with remotely sensed data and overlay tools in GIS (Beven, 2012). However, the processes at the discretization scale remain effectively lumped, but they have the advantage of being easier to implement and require significantly less computational power compared to fully distributed models (Beven, 2012).

Additionally to the topographical knowledge and impermeability factors of the landscape, data about the existing storm water drainage infrastructure is also needed. Modeling subsurface water flow in the drainage pipes, one-dimensional numerical models have

remained to be a popular solution due to their relatively simple model construction, high efficiency and shorter runtime for simulations (Chang et al., 2015). Many hydrological models, including SWMM apply one-dimensional Saint–Venant equations *(detailed explanation in Section 3.3.2)* for the calculation of flow routing within the pipes (Bates et al., 2010).

A number of currently used hydrological models such as Urban Volume and Quality (UVQ), Model for Urban Stormwater Improvement Conceptualisation (MUSIC) and Storm Water Management Model (SWMM) have also the ability to incorporate GI installations for analyzing urban storm runoff reduction (Liu et al, 2014). This is especially useful as direct measuring of how efficiently GI practices would reduce runoff is costly in terms of field and laboratory time (Zhang et al, 2015). These modeling tools allow the developer to optimize the parameters and the location for the implementation of potential GI installations such as penetrable pavements, green roofs or infiltration trenches for most effective control of urban flooding.

2.2 SWMM (PCSWMM)

The United States Environmental Protection Agency's (EPA) Storm Water Management Model (SWMM) is a dynamic hydrology-hydraulic water quantity and quality simulation model. It is used for single event or long-term (continuous) simulation of runoff quantity and quality from primarily urban areas (EPA, 2016). The source code is in the public domain, however since the early 1990s a number of derivative codes became available in the private domain, of which PCSWMM is one, which have led to the wide accessibility and popularity of the model being used for hydrological simulations (James et al., 2010; Butler and Davis, 2004).

2.2.1 Previous publications on SWMM

A large number of published papers have analyzed the advantages of using GIS for the calculation of the high number of parameter values required as an input to SWMM. GIS tools can be used for preprocessing spatially distributed input data (Han and Burian, 2009; Sun et al., 2014; Yao et al., 2016) but also for post-processing of SWMM text output files to GIS layers for enhanced visualization (Meyer et al., 1993).

Calibration and validation of the simulated results from the model is another research field has gathered much attention. Jain et al. suggest that the physical parameters (the area of the sub-catchment or the diameter and length of the pipes) can be measured directly and do not require calibration, however the hydrological parameters do need to be calibrated. As manual calibration is labour intensive, numerous automatic parameter estimation and calibration methods have been suggested (Barco et al., 2008; Baffaut et al., 1989; Liong et al., 1991). However, for larger ungauged urban areas lacking flow measurements for calibration, Kerbs et al. suggest that a feasible approach could be to use calibrated high resolution parameter values from smaller areas with similar surface types.

SWMM has also been successfully used to demonstrate the mitigating effects of storm water runoff through the implementation of Low Impact Development (LID) installations (also referred to as Green Infrastructure), such as green roofs, bioretention cells and porous pavements that promote storage, infiltration and evaporation processes (Palla et al., 2015). Porous asphalt was tested by Niemczynowicz in 1990 for the city of Lund as a LID option to combined system overflows. The author found that the peak-flow from the combined system was reduced about 75% and from the storm water system about 90%. Kim et al. also analyzed the effects of climate change and the ability of porous pavements to reduce the expected increased peak runoffs. The authors applied three design storm scenarios in SWMM depicting the rainfall intensities for current conditions, for 2020 and 2050. They concluded that porous pavement can be effective in reducing the runoff volume and peak flow below current conditions for all scenarios (Kim et al., 2015). Furthermore, Zahmatkesh et al. found that among the implemented LID types under different precipitation scenarios in New York City using SWMM, porous pavement was noted to have the greatest effect on peak flow reduction. Many experimental studies have demonstrated the positive effect of porous pavements, often first in laboratories and later on site (e.g. Dreelin et al., 2006; Fassman and Blackbourn, 2010;

Palla et al., 2015). Published papers reporting SWMM simulations with specifically porous asphalt have however remained limited.

2.3 Porous asphalt

Porous asphalt allows stormwater to infiltrate into underlying soils promoting pollutant filtering functions and recharge, as opposed to producing large volumes of rainfall runoff requiring conveyance and treatment (US EPA, 2000). Figures 2-4 illustrate just a few designs how rainwater can be removed from the surface by infiltration into the storage reservoir (Interpave, 2010). Figure 2 illustrates relatively high infiltration capacity into the subgrade. Storm water can enter the permeable sub-base (storage reservoir) and then continue the infiltration into the subgrade. It is cost efficient as drainage pipes are normally not needed (Interpave, 2010).

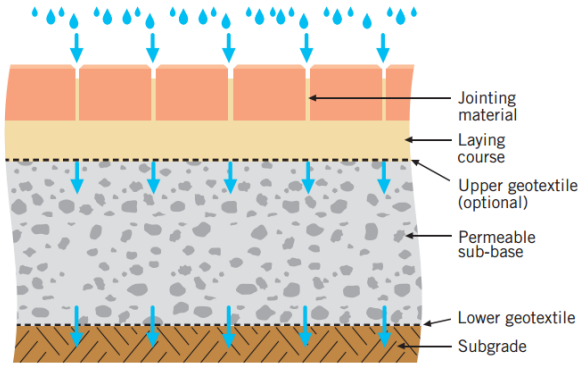

Figure 2. Full infiltration into the subgrade. Based on data from Interpave, 2010.

Storm water enters first the sub-base and then the subgrade.

Figure 3 illustrates a design where stored water in the storage reservoir is allowed to enter the drainage system through the underlying drainage pipes. It is used if subgrade has a lower infiltration capacity or to maintain stability in the subgrade (Interpave, 2010).

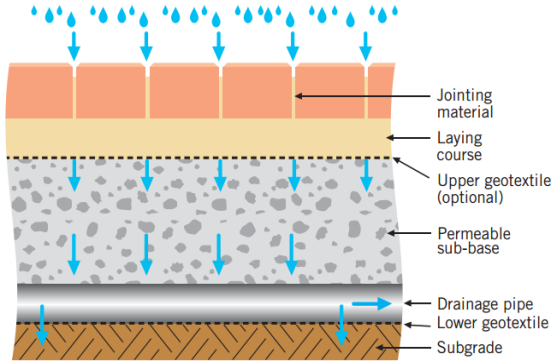

Figure 3. Partial infiltration into the subgrade. Based on data from Interpave, 2010.

Storm water enters first the sub-base and then the drainage system through the underlying pipes. There is little infiltration into the subgrade.

Figure 4 illustrates a design where the subgrade has very low permeability or where there is a high risk of contamination. Storm water infiltrates into the sub-base but further infiltration into the subgrade is prevented by the impermeable flexible membrane (Interpave, 2010).

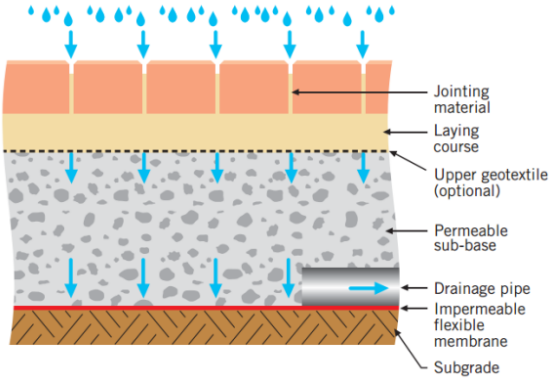

Figure 4. No infiltration into the subgrade. Based on data from Interpave, 2010.

Storm water enters the sun-grade and enters then into the drainage system through the underlying drainage pipes. Infiltration in to the subgrade is stopped by the impermeable flexible membrane.

Depending on the soil parameters, subgrade stability requirements and pollution risks, different construction methods for permeable pavement might be more suitable at different locations. For this study partial infiltration option (Figure 3) is modelled with an underdrain that allows the infiltrated water into the storage reservoir to be reintroduced to the drainage

system with a lag. The composition and structural design of the top lying porous asphalt layer can also vary depending on the surface location and use requirements. Figure 5-7 illustrate three examples of the material thickness and aggregate size suitable for varying locations.

Figure 5 shows porous asphalt minimum thickness suitable for areas with light traffic, e.g. parking lots; Figure 6 shows the thickness suitable for medium traffic, e.g. residential streets; and Figure 7 shows the thickness suitable for heavy traffic, e.g. main roads with truck traffic (FHWA, 2015).

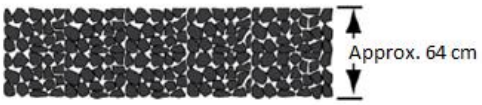

Figure 5. Porous asphalt layer thickness suitable for light traffic. Based on data from FHWA, 2015.

Figure 6. Porous asphalt layer thickness suitable for medium traffic. Based on data from FHWA, 2015.

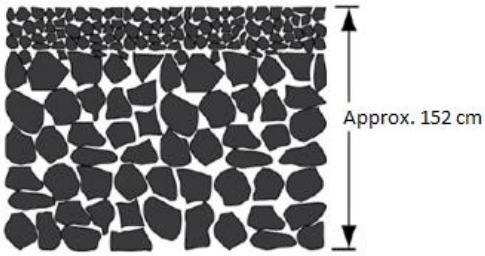

Figure 7. Porous asphalt layer thickness suitable for heavy traffic. Based on data from FHWA, 2015.

Porous asphalt is made of single-size aggregate bound together by bituminous asphalt binder, which is an inexpensive paving material (Ferguson, 2005). The aggregate, which is any mass of particulate material such as gravel, crushed stone, crushed recycled brick, or decomposed granite has to be bound together to give the mass between 16% and 22% void space (FHWA, 2015). The porous pavements are typically built over a layer of stone reservoir with 40% voids to temporarily store water as it infiltrates into the soil below (FHWA, 2015).

2.3.1 Benefits of porous asphalt

The hydrologic benefits of the use of porous asphalt have been well-documented for volume and peak flow reduction (Roseen et al., 2012). The initial infiltration capacity commonly exceeds 200 mm/min, which is more than enough for any extreme rainfall event in Sweden (Al-Rubaei et al., 2013). Based on the Swedish Water and Wastewater Association (SWWA, 2011) rainfall for a 100 year return event would have the maximum intensity of 4.0 mm/min. Beside the hydrological effects porous asphalts have also shown: (1) improved wet pavement frictional resistance, (2) reduced hydroplaning, (3) reduced splash and spray, (4) reduced nighttime glare, (5) improved nighttime pavement marking visibility, and (6) reduced pavement noise (Roseen et al., 2012).

Additionally, aggregate surfaces have been suggested to be especially applicable in areas with freezing or swelling soil types as deflections from heaving would not be noticeable on the aggregate's irregular surface (Ferguson, 2005). Furthermore, the high permeability makes the material most favorable for restoring watershed hydrology and tree rooting habitat (Ferguson, 2005).

2.3.2 Problems and solutions for porous asphalt

Although the initial infiltration capacity is extremely high, it has been proven to decrease rapidly due to surface clogging which is the primary failure mechanism for porous pavements in terms of stormwater management (Fassman and Blackbourn, 2010). Surface clogging could be caused by wind-borne dust particles, washed-on sediment, or traffic's dust and oil (Ferguson, 2005) or due to winter maintenance activities such as sanding (Putman and Kline, 2012). Additionally, Kandhal and Mallick describe that porous surfaces are prone to accelerated aging due to the oxygen access through the increased air voids - another potential clogging factor.

Several maintenance treatment methods have been suggested to increase the reduced infiltration rates and extend the life span of the surface. Winston et al. conducted an experiment at ten different porous pavement sites in the USA and Sweden to test eight different maintenance techniques. The outcome of the test showed that pressure washing,

milling[1], street sweeping (mechanical, regenerative air, and a vacuum truck) all increased or even restored the initial surface infiltration rates (Winston et al., 2016).

A limited number of long-term studies have tested the infiltration capacity decline over time. Al-Rubaei et al. conducted their study on two porous asphalts sites in Sweden with 18- and 24-year-old lifespan. The authors found that the infiltration capacity of the pavements had decreased substantially, far below initial values. However, even with the reduced rates the porous asphalt could potentially still be capable of infiltrating a 100 year return rainfall. The study concluded that 87% of such a rainfall event (with 15 min duration) would still have been infiltrated in one of the study sites, yet only 3% at the second site (Al-Rubaei et al., 2013).

3 Methods

3.1 Introduction

The aim of the study is to locate the most suitable sites for the implementation of porous asphalt within the study area (Figure 1) with the goal of reducing flooding during intense rainfall events. Sections 3.2 to 3.2.6 describe the processes in ArcMap that were used to prepare of the data for the modelling. Sections 3.3 to 3.3.3 explain the governing equations and simulation methods used in the modelling in PCSWMM. Figure 8 illustrates the workflow in ArcMap from the input data (yellow) through the processing tools (blue) for generating the three output files (red) that were consequently imported to PCSWMM. The general workflow involved using ArcMap Hydrology tools for generating the natural watersheds that cover the suggested flood prone neighborhood around Gästgivarevägen street. This watersheds were then used to cut the cadastral polygons layer and the drainage network. The imperviousness and slope percentages were also calculated for each cadastral polygon before importing them as sub catchments to PCSWMM.

[1] The process of removing at least part of the porous asphalt layer to improve permeability (EAPA, 2015)

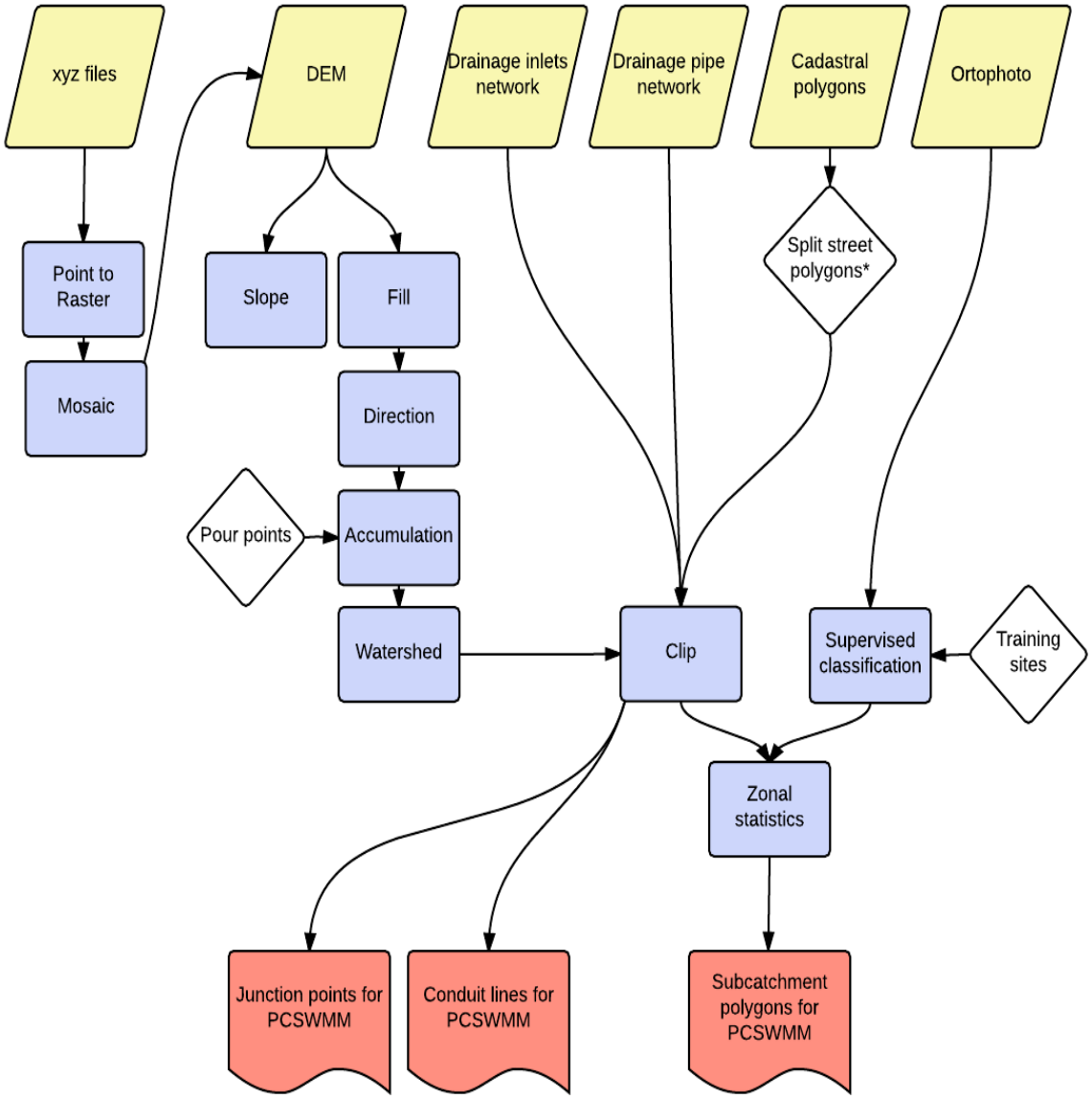

Figure 8. Workflow in ArcMap.

The input data (yellow) is processed with Arc Toolbox tools (blue) to generate three output files (red) that are consequently imported to PCSWMM.

3.2 Input data

The data for hydrological modelling in SWMM requires: high resolution DEM, land use data, soil characteristics, hourly (or sub-hourly) rainfall data, sewer system network map and storm sewer discharge data for calibration and validation

3.2.1 DEM

High resolution elevation data was obtained from the Lund Municipality City Planning department (Stadsbyggnadskontoret). The data was received as .xyz files previously interpolated (regularly spaced) with the resolution of 1 meter with the height accuracy of 0.05 m in the coordinate system of SWEREF99 13 30 (GSD, 2015). In total of 27 files with 250 000 points in each file were first converted in Excel to .txt format before importing them to

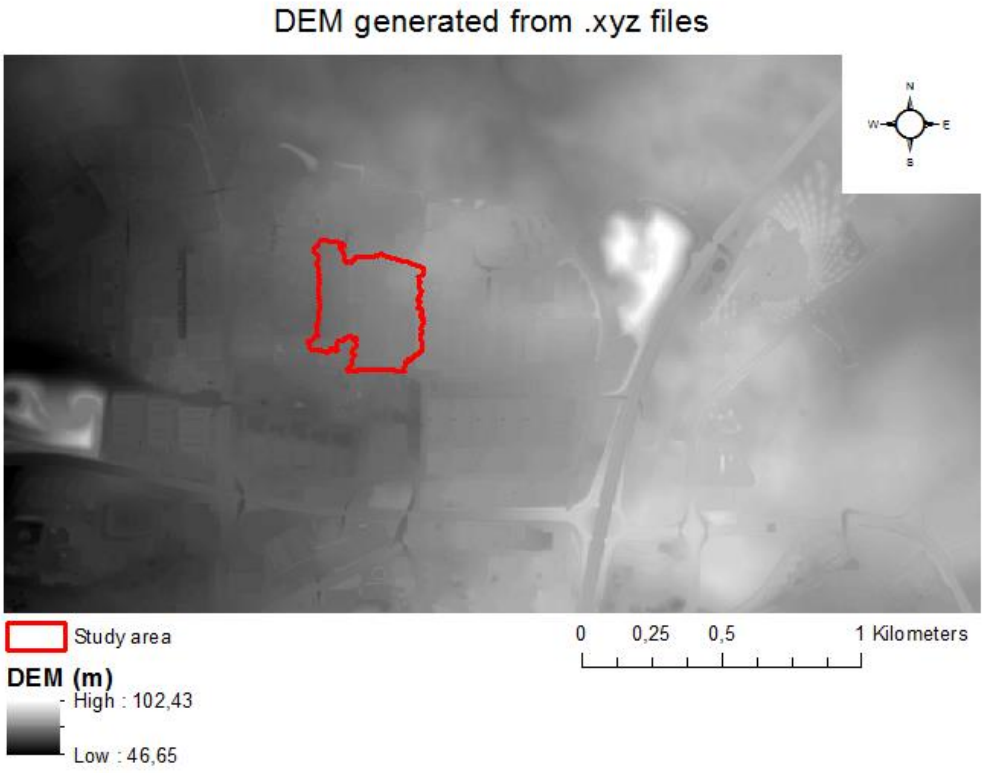

Figure 9. DEM generated of the study area.

The DEM was generated from .xyz files received from the Lund Municipality City Planning department. 27 files were first converted from point to raster layers and consequently fitted together with the Mosaic tool in ArcMap.

ArcMap. In ArcMap the Conversion tools were used to convert the .txt file to .dBase format. All the files in the .dBase format were added to ArcMap as new Event layers which were consequently transformed from point to raster layers and joined together with the Mosaic tool. The study area was then delimited according to the boundary of the watersheds covering the neighborhood around Gästgivarevägen street. The watersheds were calculated with ArcMp Hydrology Tools using the newly generated DEM. Tow pour points were added according to

the accumulated flow streams (Figure 13) to delineate the watersheds that would cover the study area. Figure 10 shows the extent of the two watersheds that were joined together to clip out the study area from the cadastral property units layer.

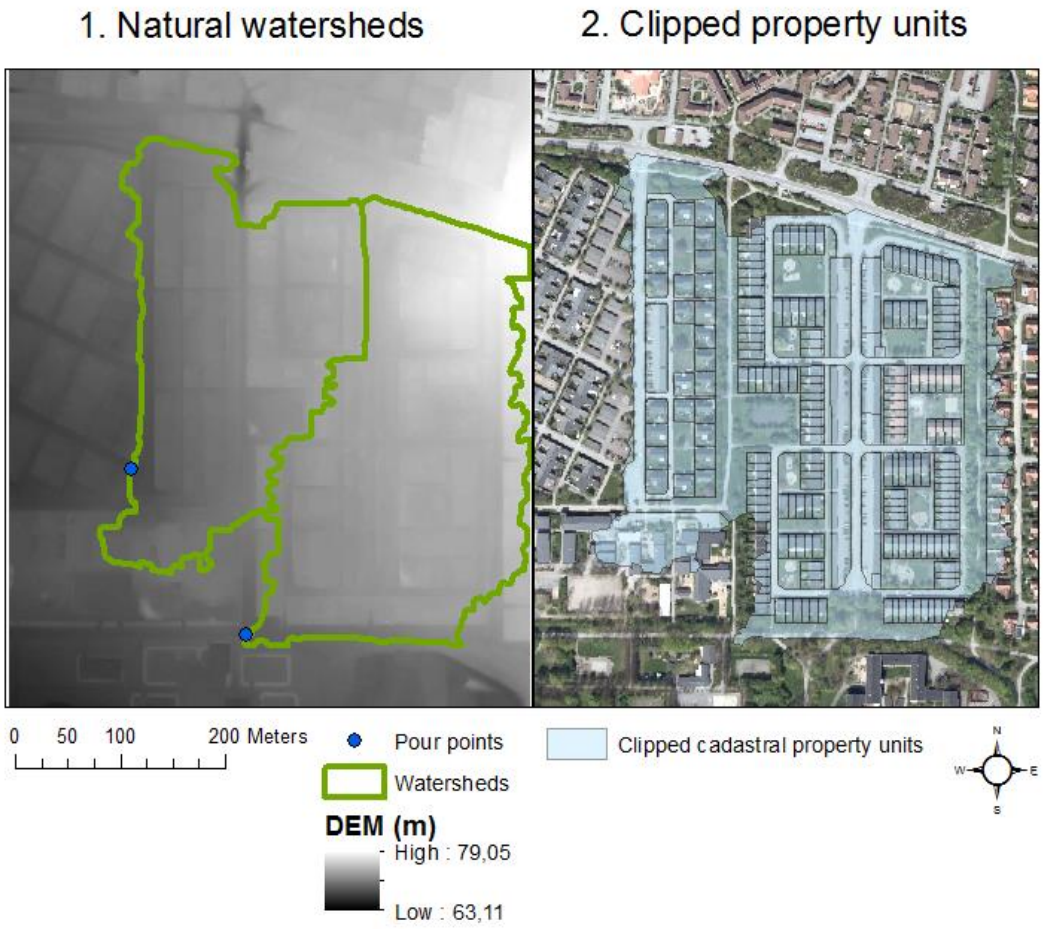

Figure 10. Study area according to the generated watersheds based on the DEM.

The first image shows the extent of the two watersheds with the location of pour points that receive the highest accumulation of surface flow. The second image illustrates the cadaster property units cut out according to the dimension of the natural watersheds.

3.2.2 Cadastral property units

The cadastral property units layer was received from Lantmäteriet in vector format in the coordinate system of SWEREF 99 TM. The data has a 2 meter mean error of location accuracy of the mapped objects. Unlike the property units with definite boundary, the roads are represented in the same shape file by continuous polygons that had to be further

subdivided into smaller sub-catchment areas. Thiessen polygons, as suggested by Jain et al. were created around each inlet to split up the large polygons representing the continuous streets.

3.2.3 Ortophoto

The ortophoto used for the study was received from Lantmäteriet with 1 meter resolution in the coordinate system of SWEREF 99 TM. The image had three visible bands (red, green, blue). ArcMap ENVI Image Processing tools were used to classify the land into two categories: pervious and impervious (Figure 11). Supervised classification was used with training sites belonging to 4 classes (grass, trees, roofs and streets). Consequently, the pervious areas were reclassified as 0 and impervious as 1. ArcMap Zonal statistics tool under Spatial Analyst Tools was then used to calculate the percentage of impervious areas for each cadastral polygon.

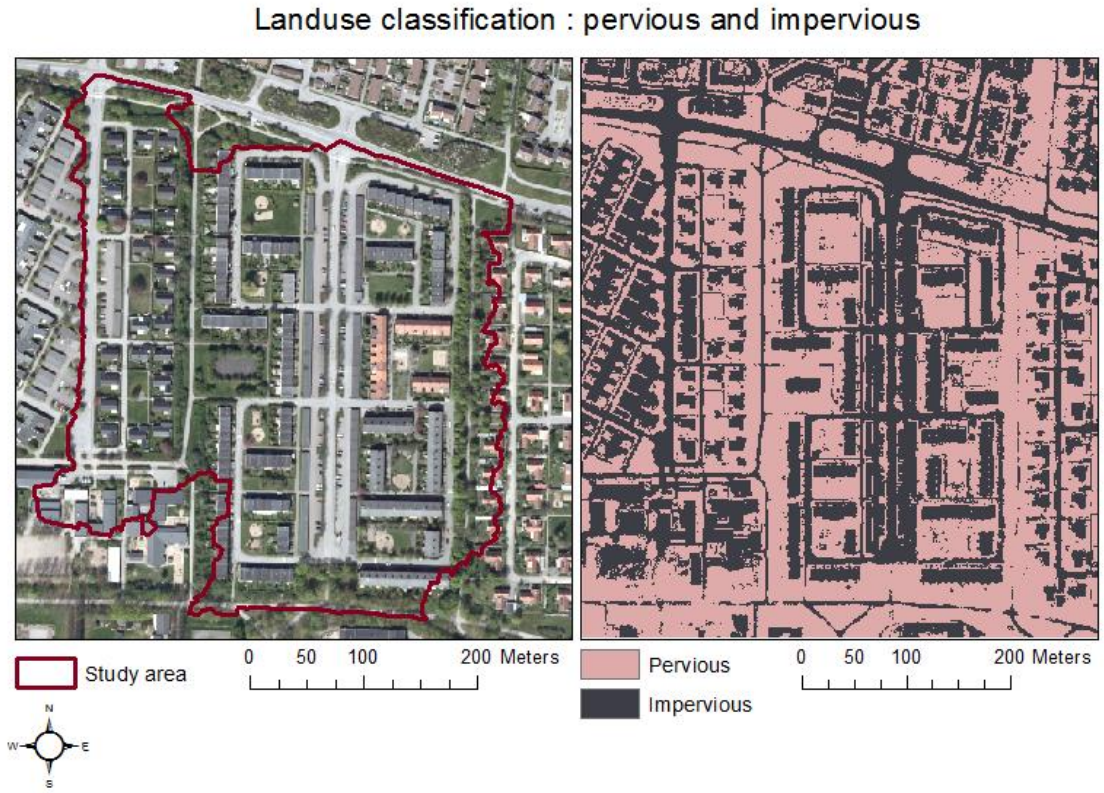

Figure 11. Land use classification for the study area.

The land use within the study area was classified into two classes: impervious (gray) and pervious (pink). Impervious class includes areas under streets and buildings. Pervious class includes areas under grass and trees.

3.2.4 Soil

Detailed data of the soil types for the study area was lacking, however the attributes were estimated based on the information provided by two web-based geodata services: the Open Geodata Portal, managed by the National Land Survey (Lantmäteriet) and the County Board (Länsstyrelsen). The first classifies the soil type under the study area as fine clay moraine (Moränfinlera) and the second database provides information about the clay content of the surrounding arable areas. The clay content north from the study area (approximately at a distance of 200-300 m) varies between 20-30%. According to the USDA soil texture classes, widely used also in Europe for estimating soil properties based on the clay, silt and sand content (Ballabio et al., 2016) clay loam was estimated to be the dominant type in the study area (USDA, 2016). The soil characteristics for the modelling in PCSWMM were set according to the values for the soil type of sandy clay loam suggested by Rawls et al. (as cited in James et al., 2010). Table 1 provides the soil infiltration parameters used for the study.

Table 1. Soil infiltration characteristics Rawls et al., 1983 (as cited in James et al., 2010).

	K	Ψ	Φ
Sandy Clay Loam	1.524	219.964	0.398

where

K = saturated hydraulic conductivity, mm/hr

Ψ = suction head, mm.

Φ = porosity, fraction

3.2.5 Rainfall

The rainfall events used for the simulations were 30 min blocks with mean rainfall intensities for 1, 10, 50 and 100 year return events. The mean intensities were based on the published data by Svenskt Vatten (Swedish Water service company) for Lund Municipality for the duration of 5-120 min (VA Syd, 2012). Table 2 has the intensity figures in mm/hr for the 4 return period events for 5 to 120 min duration of which the 30 minute intensities were used for the modelling in PCSWMM.

Table 2. Simulated mean rainfall intensities for 30 min events for 1, 10, 50 and 1100 year rainfall events.

Rainfall intensities (mm/hr) of various rainfall durations (5-120 min) and return periods (1-100 years).

	5min	10min	15min	20min	**30min**	60min	90min	120min
1 year	52,776	38,484	30,564	25,632	**19,728**	12,312	9,288	7,596
10 year	112,86	82,08	65,016	54,36	**41,652**	25,704	19,188	15,516
50 year	192,492	139,824	110,664	92,484	**70,74**	43,452	32,292	26,064
100 year	242,352	175,968	139,248	116,316	**88,92**	54,54	40,5	32,616

3.2.6 Drainage network

The stormwater drainage network consisting of pipes and manholes was received in shape files from VA Syd in the coordinate system of SWEREF99_13_30. The interconnecting pipes, represented as lines had attribute information concerning the unique ID of the upstream and downstream manholes, offsets from the ground level, roughness, slope, shape and diameter of the pipe. The manholes, represented as points had attributes with their unique ID, size and cover level. This interconnected system was used as the core drainage network, however the manholes represented are covered inlets where the storm water runoff does not enter in reality. Therefore, one day of field work was used to gather the location and elevation data of all of the open inlets in the study area. Topcon's GRS-1 (Geodetic Rover System) with integrated dual constellation network, GPS (Global Positioning System) and GNSS (Global Navigation Satellite System) rover system was used for the data collection. Thanks to the Network RTK (real time kinematic) service (SWEPOS) measurement corrections can be reduced in real time to centimeter level. The horizontal and vertical accuracy during the field work stayed always under 20 cm, often as low as 1-2cm (Appendix 1, Pictures 1-2). The majority of those open inlets were not managed by VA Syd and therefore they lacked data concerning their location, invert levels and how they are connected to the rest of the drainage system. During the data collection at the study area some of the inlets were opened and the invert elevation was measured. However, many of the inlets could not be opened as they were bolted down (Appendix 1, Picture 5) or the elevation could not be measured because the bottom could not be reached due to accumulated sediment (Appendix 1, Picture 3-4). Based on the measurements taken a general assumption was made to give the inlets an invert elevation of 2 meters from the measured cover level height. Additionally, the inlets were connected to the closest existing pipes with an estimated 0.225 meter diameter. The inlets that did not align an existing pipe line but followed a line pattern were first connected with 0.225 meter diameter pipe with the direction according to natural slope before connecting them to the existing pipe network.

3.3 PCSWMM simulation

PCSWMM is built upon EPA SWMM 5 operating on a collection of subcatchment areas that receive precipitation and generate runoff, which can be further routed to adjacent

subcatchments or transported to interconnected drainage system represented by pipes, channels, storage and treatment devices, pumps, and regulators (James et al., 2010). For each subcatchment the quantity and quality of runoff is calculated and for the drainage pipes the water flow rate and volume are calculated. Figure 12 illustrates the spatial set up for the study area modelled. It consists of 440 subcachments, 284 junctions, 284 conduits (pipes) and 2 outfall nodes.

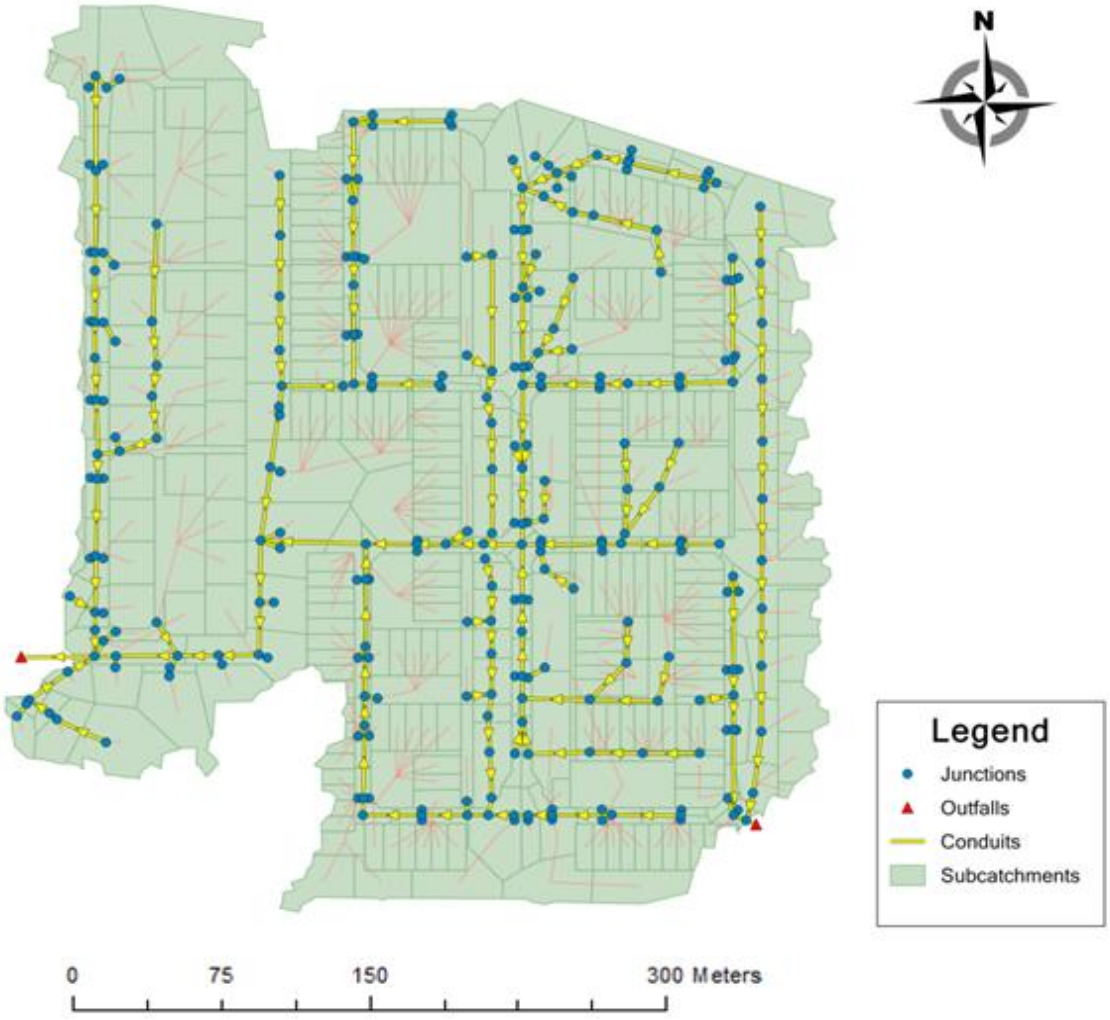

Figure 12. PCSWMM model of the study area.

The area consists of cadastral property units as Subcatchments (green), inlets as Junctions points (blue), connecting pipes as Conduit lines (yellow) and two outfalls of the drainage system (red).

3.3.1 Rainfall – runoff calculation

The outflow of each subcatchment is calculated based on the inflow that includes the precipitation and outflow from upstream subcatchments. The losses include infiltration, evaporation and depression storage.

1. The surface runoff (if the subcatchment width, W is known) is calculated by Manning's equation (1) (James et al., 2010):

For overland flow:

$$\boldsymbol{Q = W\frac{1.0}{n}(d - d_p)^{5/3}S^{1/2}} \quad (1)$$

where

W = subcatchment width, m,

n = Manning's roughness coefficient,

d_p = depth of depression storage, m, and

S = subcatchment slope, m/m.

For flow in drainage pipes:

$$\boldsymbol{Q = \frac{1.0}{n}AR^{2/3}S^{1/2}} \quad (2)$$

where

W = subcatchment width, m,

n = Manning's roughness coefficient,

A = cross-sectional area, m^2,

R= hydraulic radius, m and

S = subcatchment slope, m/m

2. Infiltration loss into the pervious subcatchments areas can be calculated using Horton's Equation, Curve Number or Green-Ampt Method. The latter was chosen in this study, which uses the two-stage Mein-Larson formulation (3). The first step predicts the volume of water which will infiltrate before the surface becomes saturated (F_s). Clay soils, which are the dominant type in the study area have a very low saturated hydraulic conductivity (K_s) and therefore the cumulative infiltration volume (F_s) to cause surface saturation is relatively small. Once the surface saturation has been reached, succeeding infiltration capacity is predicted by the Green-Ampt equation. It calculates the infiltration capacity (f_p) by taking into account the infiltrated volume (F), which in turn depends on the infiltration rates in previous time steps (James et al., 2010). Due to the very slow infiltration rates clay soils have a very high runoff potential.

Thus:

For $F < F_s$:

$$\mathbf{F_S} = \frac{\boldsymbol{S * IMD}}{\frac{\boldsymbol{i}}{\mathbf{K_S}} - \mathbf{1}} \tag{3}$$

$$f = i$$

for $i > K_s$

No calculation of F_s *for* $i <= K_s$

For $F >= F_s$:

$$f = f_p \quad \textit{and}$$

$$\mathbf{f_p} = \mathbf{K_s}(\mathbf{1} + \frac{\mathbf{S * IMD}}{\mathbf{F}})$$

where

f= infiltration rate, mm/hr,

f_p= infiltration capacity, mm/hr,

i= rainfall intensity, mm/hr,

F= cumulative infiltration volume, this event, mm,

F_s= cumulative infiltration volume required to cause surface saturation, mm,

S= average capillary suction at wetting front, mm,

IMD= initial moisture deficit for this event, frac., and

K_s= saturated hydraulic conductivity of soil, mm/hr.

3. Evaporation loss would be calculated for standing water on subcatchment surfaces set by the depression storage parameter, subsurface water in groundwater aquifers and for water held in storage units based on inserted temperature data. Evaporation would influence the water volume during long-term runoff simulation, specifically during dry periods, however for this study simulating single events, evaporation was not considered to be an influential parameter.

3.3.2 Water routing from subcatchments

Water from subcatchments can be routed through the drainage network using one of the three methods: Steady Flow, Kinematic Wave or Dynamic Wave Routing. The latter is the most powerful solving the complete one-dimensional Saint Venant flow equations. The equations consist of the continuity (4) and momentum equations (5) for conduits and a volume continuity equation at nodes. Dynamic Wave Routing was also use for this study.

1. The continuity equation (James et al., 2010):

$$\frac{\partial A}{\partial t} + \frac{\partial Q}{\partial x} = 0 \qquad (4)$$

where[2]

A = cross sectional area,
Q = conduit flow,
x = distance along the pipe, and
t = time.

2. The momentum equation:

$$\frac{\partial Q}{\partial t} + \frac{\partial (\frac{Q^2}{A})}{\partial x} + gA\frac{\partial H}{\partial x} + gAS_f = 0 \qquad (5)$$

[2] If metric units are used, flow is in m^3/sec. These units are carried through internal calculations as well as for input and output.

where

g = gravitational constant,
H = z + h = hydraulic head,
z = invert elevation,
h = water depth, and
Sf = friction slope.

The Dynamic Wave routine is a hydraulic flow routing model receiving hydrograph input at specific nodal locations, which are then routed through the storm drainage system to the final outfalls. For the dynamic wave routine, the momentum equation is combined with the continuity equation to yield an equation to be solved along each link at each time step.
Thus:

$$\frac{\partial Q}{\partial t} + gAS_f - 2V\frac{\partial A}{\partial t} - V^2\frac{\partial A}{\partial x} + gA\frac{\partial H}{\partial x} = 0 \qquad (6)$$

where

Q = discharge along conduit,
V = velocity in the conduit,
A = cross sectional area of the flow,
g = gravitational constant,
H = hydraulic head, and
S_f = friction slope.

3.3.3 LID simulation

LID (low impact development) practices can be modeled in PCSWMM by assigning a set of predesigned LID controls to the subcatchment. The LID Control Editor allows the simulated porous asphalt to be assigned various parameters for the surface, porous pavement, subsoil, storage reservoir and an existing underdrain. The porous asphalt for the simulation was designed to have a high permeability representing a newly laid pavement, an underdrain and an option of two storage thicknesses of 0.5 meters and 0.25 meters. Table 3 lists the parameters used for porous asphalt.

Table 3. Porous asphalt parameters used for the modelling.

	Berm height mm	Surface roughness	
Surface	20	0.02	
	Thickness mm	Void ratio	Permeability mm/hr
Pavement	150	0.21	2000
	Thickness mm	Void ratio	Seepage rate mm/hr
Storage	500 or 250	0.75	1.5
	Drain coefficient mm/hr	Drain exponent	Drain offset height mm
Underdrain	0.2	0.5	30

The location of the porous asphalt was decided based on the accumulated flow streams and the highest flooded nodes. The accumulated flow streams were generated in ArcMap using the 1 meter resolution DEM. The flooding nodes were located using PCSWMM simulation (Figure 16). Polygons with porous asphalt were located on streets that had 7 out of 11 top highest flooding nodes and along streets with accumulated flow streams belonging to all 4 classes. The aim was to select areas that would most effectively reduce flooding at the southern downstream areas known to have been previously affected during intense rainfall events. Initially only upstream areas based on stream accumulation not overflow from inlets were selected to see how upstream surface change could prevent or reduce the southern downstream flooding risk. However, the model allows surface runoff to be routed only to an inlet or to another subcathment. For this study all of the surface runoffs that had inlets located within their polygons were directed there to enter the drainage system. In case the inlet overflows, excess water is not tracked down as it might move from upstream to downstream areas, but simply accounted for in the final status report and removed from the system. Only, in case of the added LID practice the water from a flooding inlet is directed to the polygon with porous asphalt that is located around or adjoining the inlet.

Figure 13 shows the accumulated flow streams segmented into 4 classes based on their increasing volumes and the final location of the streets changed for porous asphalt. The size of the area for porous asphalt for each selected polygon was calculated based on the percentage under impervious land cover of that polygon. Therefore, only paved areas and not permeable areas (e.g. grass) were changed.

Additionally, overflow from inlets in PCSWMM that has not been routed to another polygon or LID practice is lost from the system and is counted as flooding. To allow the water from flooding inlets to be routed to the area of porous asphalt where it could be absorbed into the reservoir storage and then reintroduced to the drainage system, links called Weirs were used. Weirs in PCSWMM behave as open channels that were used in this study to simulate the movement of the water from the flooding inlet onto the porous asphalt pavement. Excess water was only routed from the flooding inlets located inside the polygon with porous asphalt or flooding inlets located from adjacent polygons located upstream from the polygon with porous asphalt.

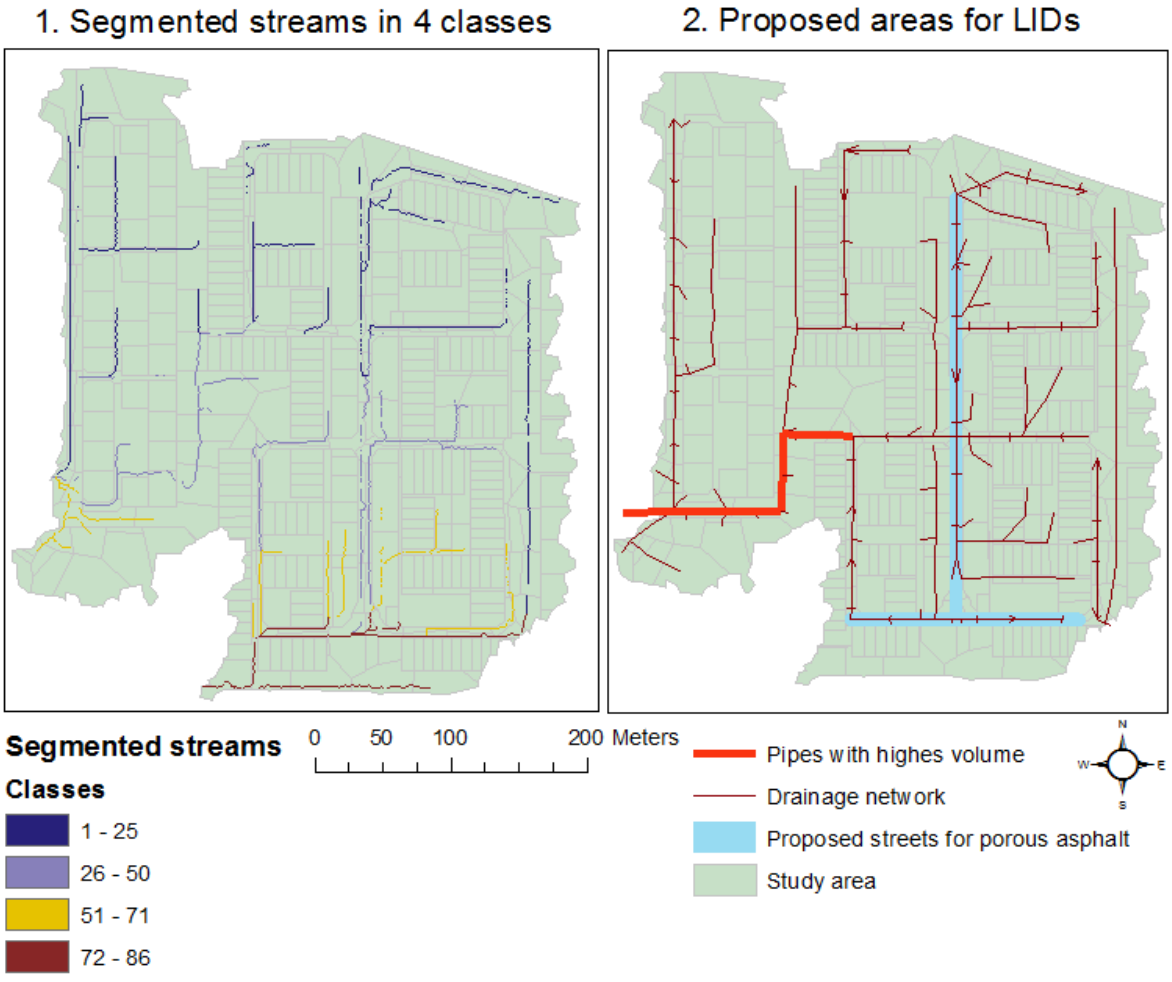

Figure 13. Selected street areas for porous asphalt implementation based on stream accumulation and drainage volumes.

Image 1 illustrates flow accumulation streams segmented into four classes based on their accumulated volumes, generated in ArcMap. Image 2 illustrates the drainage network with the sections with highest volumes, modelled in PCSWMM, highlighted in bold red. The selected streets for the implementation of porous asphalt in PCSWMM are highlighted in blue.

4 Results

4.1 Before the implementation of porous asphalt

Initially the model was run 4 times using the different rainfall event scenarios with 1, 10, 50 and 100 year return rainfall intensities. These results were considered as the 'No Change' events that consequently could be compared with the simulation results after the implementation of porous asphalt. Two types of porous asphalt designs were implemented at separate times with storage layer thickness for the gravel reservoir of 0.5 meters and 0.25 meters. This was simulated to estimate the impact of the thickness of the storage layer on reducing the water volume at the downstream end of the study area.

The output of each model run is a status report that summarizes the runoff quantity and flow routing continuity errors, followed by a detailed report for each subcatchment, junction (inlet), conduit (pipe) and LID practice. The runoff continuity error is calculated based on the difference between the input volume of water (rainfall) and the output volume (e.g. flooding, storage, infiltration) within each subctchment. The routing continuity error matches the input water volume entering the drainage system with the outfall volume. It takes into account losses due to flooding and final storage inside the pipes after the 30 minute simulation event (see Appendix 2 for an example of the top of the status report). For all of the final 12 simulations (4 times 'No Change', 4 times '0.5m porous asphalt' and 4 times '0.25m porous asphalt') the runoff continuity error stayed less than 5.182% and the flow routing error remained less than 3.198%. It is suggested that for errors over 10% for both should not be considered unacceptable and the validity of the analysis results should be questioned (James et al., 2010).

Figure 14 illustrates the flooding results for the whole study area for all of the 'No Change' scenarios. The top graph is plotted with the 4 different rainfall event intensities for the duration of 30 minutes, simulated with 5 minute time steps. The second graph shows the flooding intensity following the 4 rainfall events. The total amount of flooding is recorded to be 142.9 m^3, 869.8 m^3 and 1607 m^3 for the 10, 50 and 100 year events respectively. No flooding is recorded for the 1 year return rainfall event.

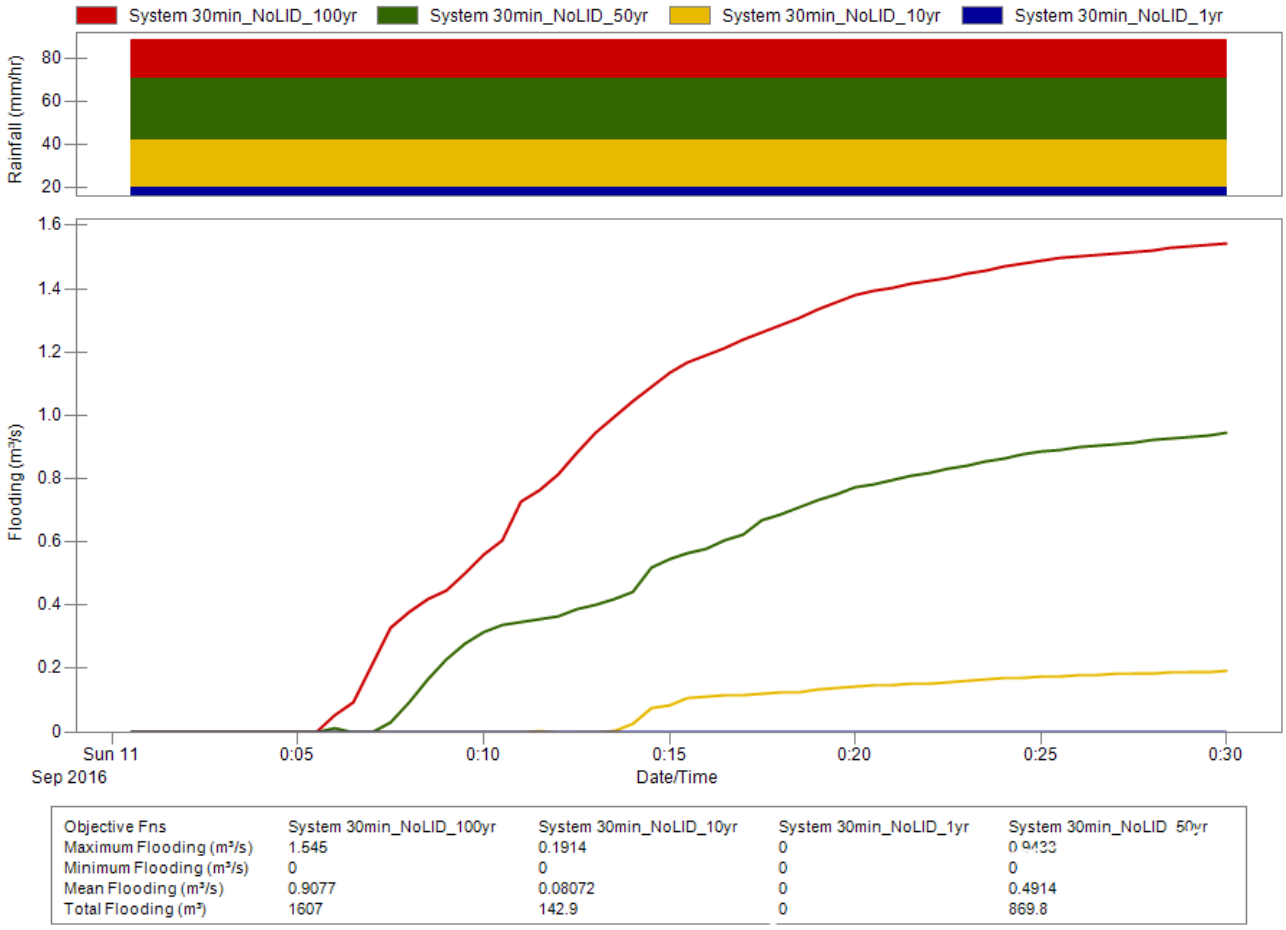

Objective Fns	System 30min_NoLID_100yr	System 30min_NoLID_10yr	System 30min_NoLID_1yr	System 30min_NoLID_50yr
Maximum Flooding (m³/s)	1.545	0.1914	0	0.9433
Minimum Flooding (m³/s)	0	0	0	0
Mean Flooding (m³/s)	0.9077	0.08072	0	0.4914
Total Flooding (m³)	1607	142.9	0	869.8

Figure 14. Rainfall and flooding for 4 simulated rainfall events.

The upper graph shows the simulated rainfall intensities for 1, 10, 50 and 100 year return events (mm/hr). The second graph below depicts the flooded volumes for the 30 minute rainfall events (m^3/s).

Flooding occurs once the horizontal drainage pipes get filled with water and further oncoming water pushes the water level in the vertical pipes above the cover level of the inlet. Figure 15 illustrates a flooding node (Junction J21) during the simulation. The profile graph shows the underground pipes and the connecting inlets with their rim levels at the ground elevation. The ground distance is on the x-axis and elevation on y-axis. When flooding occurs it is shown with a red circle and the water volume that overflows is accounted for and removed from the system.

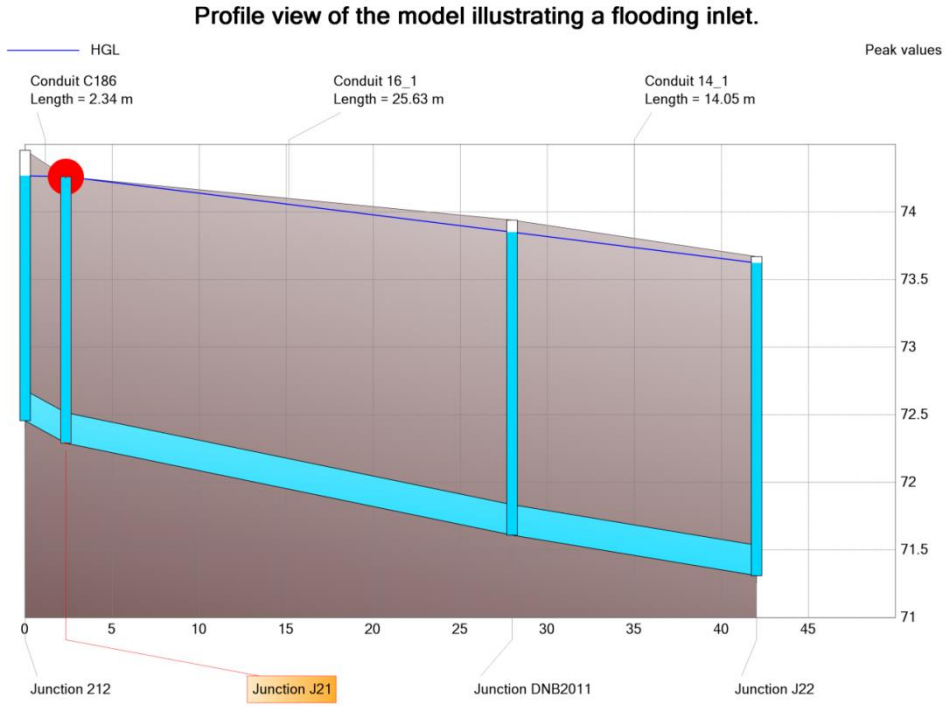

Figure 15. Profile view of a flooding inlet (Junction J21).

The ground elevation is shown on the y-axis and filled in the graph with brown colour. The x-axis depicts the distance. Junctions 212, J21, DNB2011 and J22 are connected with Conduits C186, 16_1 and 14_1. The red circle illustrates a flooding node (J21). HGL (hydraulic grade line) shows the level of water in the inlet pipes during the simulation event.

Inlets most at risk of flooding based on the 100 year rainfall return event scenario are shown in Figure 16. The total flooding volume among all of the inlets varies from 0 to 0.248 ML. A threshold of 0.054 ML was chosen to bring out the top eleven inlets with highest flooded volume, which are depicted with red color and enlarged circles. The top three inlets (no. 153, no. 149 and J5) with the highest flooding volumes (247.8 m^3, 130.8 m^3 and 114.7 m^3) were located on the streets selected for the implementation of porous asphalt (Gästgivarevägen street and southern ends of Vapenkroken and Källarekroken streets). In combination these three inlets caused approximately 31% of the total flooding volume for the whole study area during the 100 year return rainfall event.

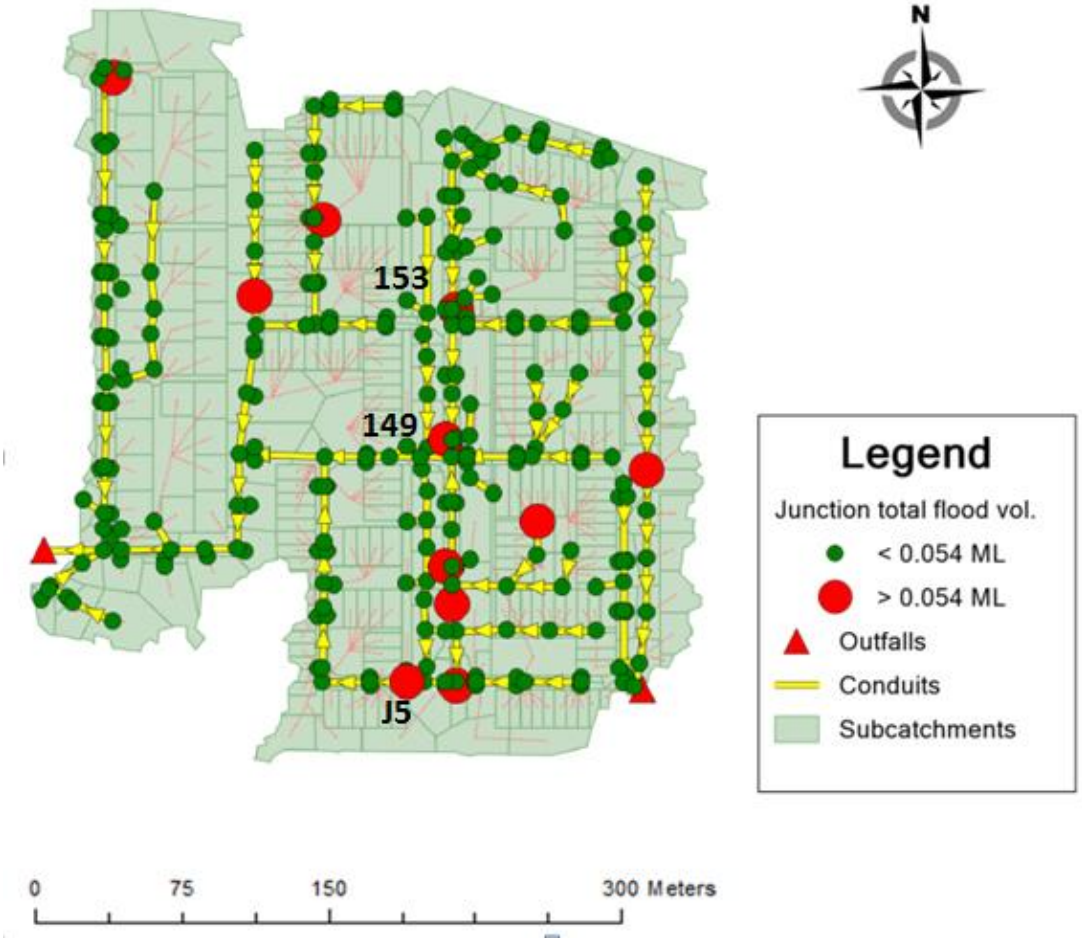

Figure 16. Inlets with highest volumes of flooding for 100 year return rainfall event.

A threshold value of 0.054 Megaliters was chosen to bring out the top ten flooded inlets. Inlets no. 153, no. 149 and J5 are the inlets that flooded the most.

Figure 17 illustrates the flooding volumes for the top three nodes (no. 149, no. 153 and J5). Node 149 has a total flooding water volume of 247.8 m^3, Node 153 has 130.8 m^3 and Node J5 has 114.7 m^3 during the 30 minute rainfall events.

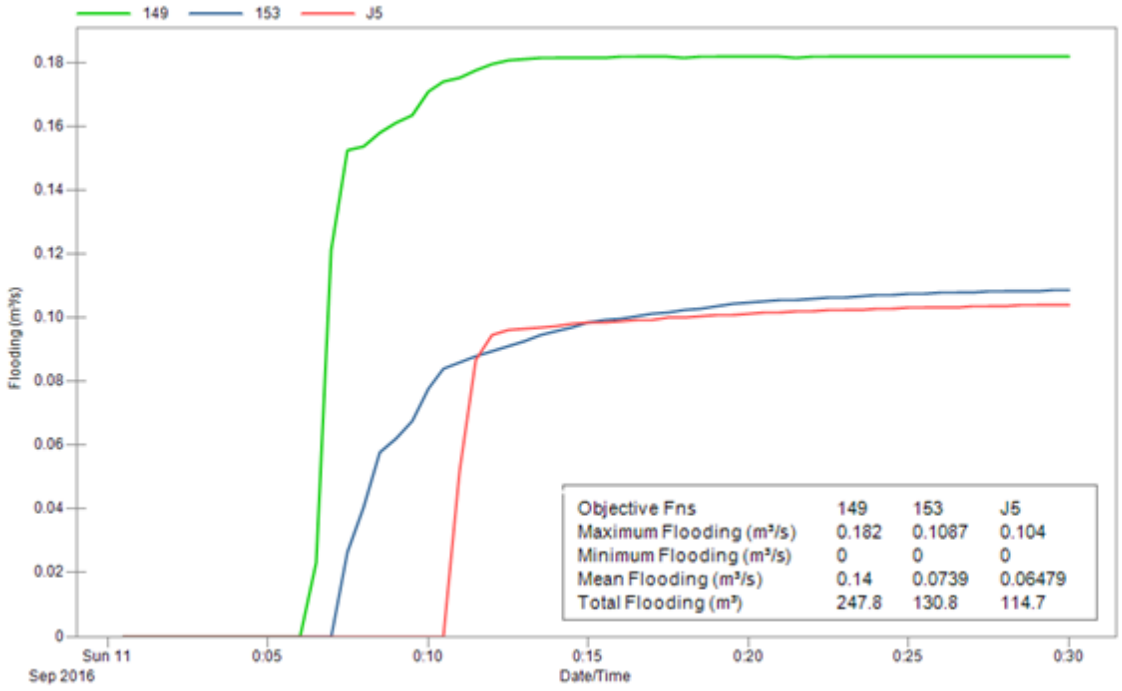

Figure 17. Flooding of the three nodes with the highest volumes (149, 153, J5) for 100 year return rainfall event.

4.2 After the implementation of porous asphalt

After the implementation of porous asphalt the total flooding in the study area did decrease significantly. Figures 18 to 20 illustrate the reduction of flooding over the whole area for the 100, 50 and 10 year return rainfall events. The 'No Change' scenario without porous asphalt is depicted with a black line and the scenarios with 0.5 meters and 0.25 meters porous asphalt results are in shades of green and red. Increasing the reservoir thickness had a very limited impact on further reducing the overall flooding. Table 4 brings out the flooding volumes for the different scenarios and the reduced percentage of the flooded water volumes compared to the 'No Change' scenario. The implementation of porous asphalt completely eliminated flooding for the 1 year return rainfall event; 0.25 meter porous asphalt design reduced flooding 65.6%, 77.5% and 99.2% for the 100, 50 and 10 year return rainfall events. Further increasing the storage capacity did not further reduce flooding for the 10 and 50 year return rainfall events and only decreased it by 0.4% for the 100 year return event.

Table 4. Flooding reduction after porous asphalt implementation.

Rainfall event	**Total flooding m^3**				
	No porous asphalt	**0.5 m porous asphalt**	Reduced percentage	**0.25 m porous asphalt**	Reduced percentage
100 yr rainfall	1607	547	**66**	553.5	**65.6**
50 yr rainfall	869.8	195.4	**77.5**	196	**77.5**
10 yr rainfall	142.9	1.2	**99.2**	1.2	**99.2**
1 yr rainfall	0	0	**NA**	0	**NA**

Porous asphalt was implemented to 29 polygons for the portion of impermeable areas that depicted the paved streets of Gästgivarevägen street and southern ends of Vapenkroken and Källarekroken streets as was shown in Figure 13. The total area under the designed porous asphalt in the modelling was 4370 m^2. The porous asphalt for the study was designed to allow

infiltration also into the underlying drainage pipe, which increases the total water volume that could be stored during the 30 minute rainfall simulation. The total volume passing through the storage reservoir depends however on the available rainfall intensity, flooded water to the porous pavement and the capacity of the underlying drainage to reduce the existing volume in the reservoir.

Figures 18-21 illustrate the reduction of flooding during the 10, 50 and 100 year return rainfall events. The significant flood volume reduction in percentages is shown in Table 4. However, the minimal difference after increasing the stone reservoir thickness from 0.25 meters to 0.5 meters will be further analysed in the discussion part.

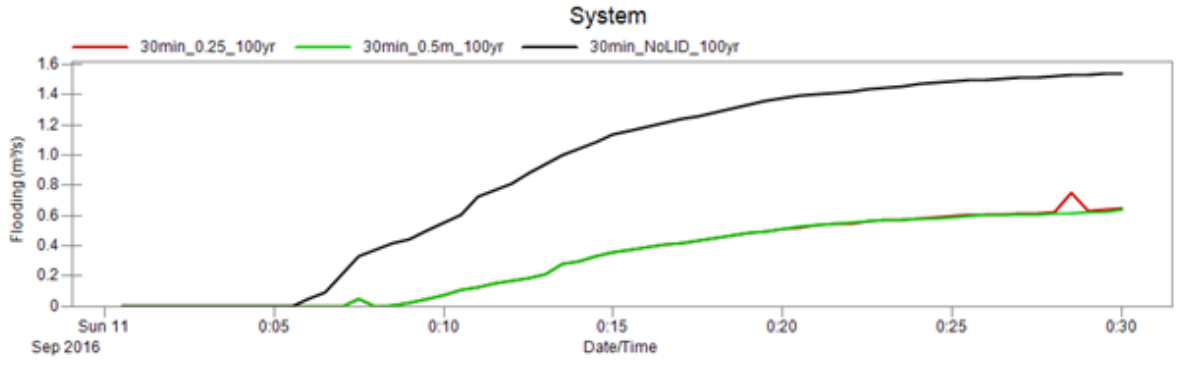

Objective Fns	System 30min_0.25_100yr	System 30min_0.5m_100yr	System 30min_NoLID_100yr
Maximum Flooding (m³/s)	0.7524	0.6377	1.545
Minimum Flooding (m³/s)	0	0	0
Mean Flooding (m³/s)	0.3127	0.3091	0.9077
Total Flooding (m³)	553.5	547	1607

Figure 18. Flood reduction for 100 year rainfall event.

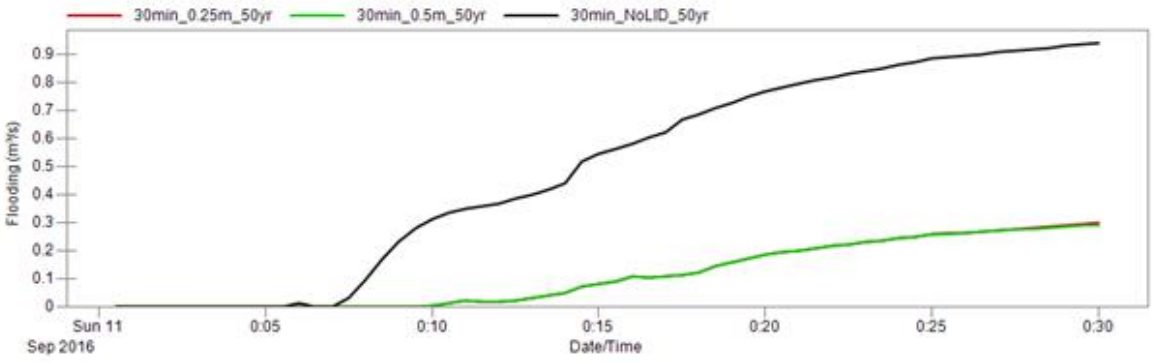

Objective Fns	System 30min_0.25m_50yr	System 30min_0.5m_50yr	System 30min_NoLID_50yr
Maximum Flooding (m³/s)	0.2975	0.2919	0.9433
Minimum Flooding (m³/s)	0	0	0
Mean Flooding (m³/s)	0.1107	0.1104	0.4914
Total Flooding (m³)	196	195.4	869.8

Figure 19. Flood reduction for 50 year rainfall event.

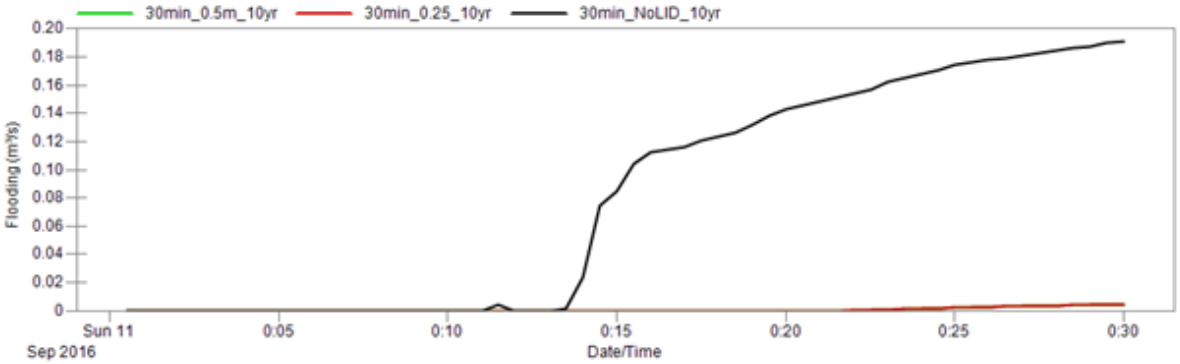

Objective Fns	System 30min_0.25_10yr	System 30min_0.5m_10yr	System 30min_NoLID_10yr
Maximum Flooding (m³/s)	0.004621	0.004623	0.1914
Minimum Flooding (m³/s)	0	0	0
Mean Flooding (m³/s)	0.0006777	0.000678	0.08072
Total Flooding (m³)	1.199	1.2	142.9

Figure 20. Flood reduction for 10 year rainfall event.

A selection of three subcatchemnts, one located upstream of the study area (no. 1304), in the middle part (no. 1301) and one in the downstream section (no. 1324) were selected for detailed analysis for the porous asphalt reservoir capacity. Figure 21 illustrates the location of the selected street sections for the implementation of porous asphalt in the model.

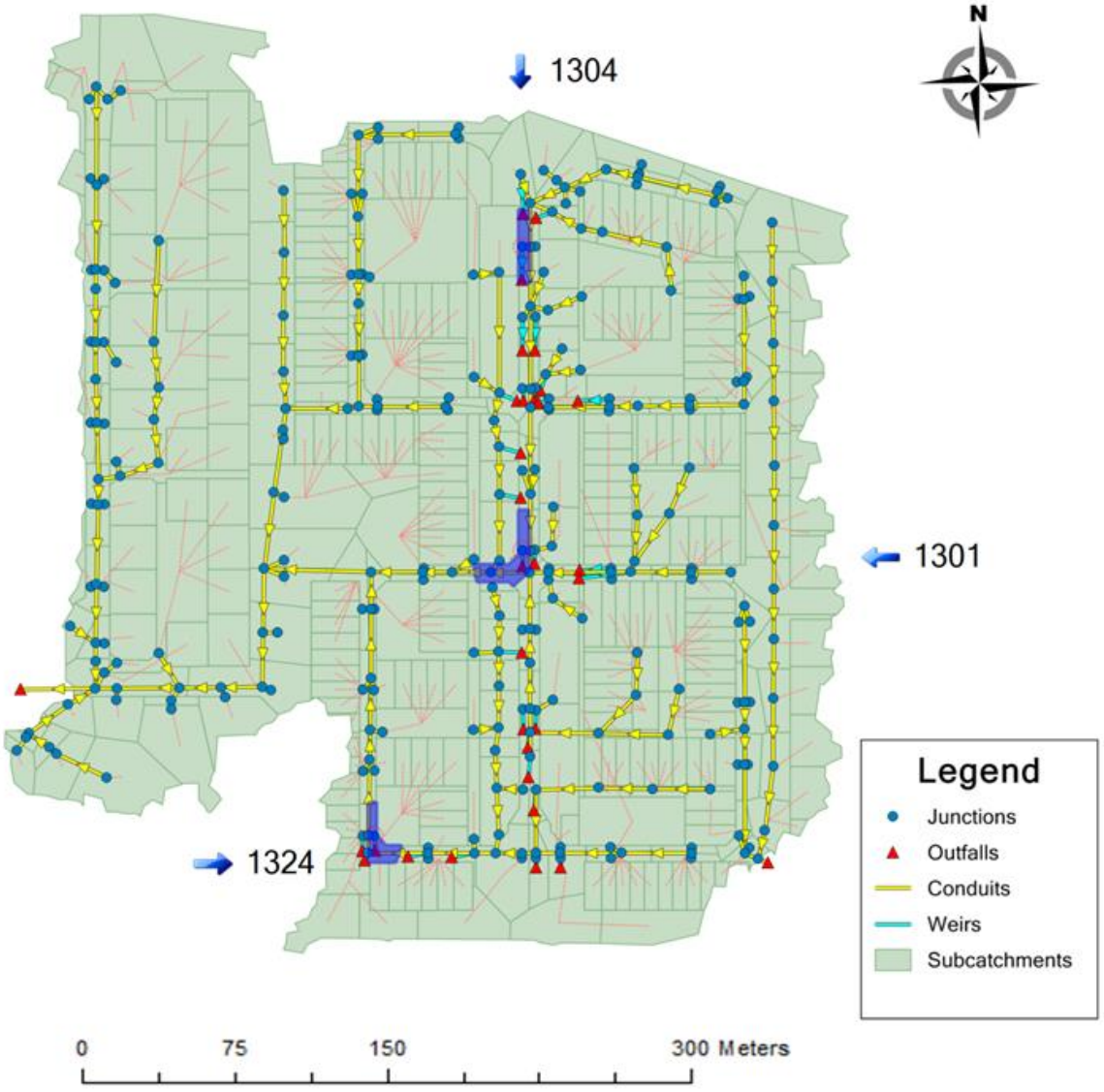

Figure 21. Selected subcatchments for porous asphalt capacity analysis (no. 1301, no. 1304, no. 1324).

Porous asphalt reservoir capacity is never exceeded during the 1 and 10 year return rainfall simulations. Table 5 brings out the time after the start of the simulation before the store reservoir reaches its maximum capacity and further water is prevented from entering the

porous pavement. Porous asphalt design for the upstream section (polygon no. 1304) with 0.25 (and also 0.5) meter reservoir thickness is suitable to absorb all of the excess water for all of the rainfall intensity events. During the 50 year return rainfall event porous asphalt storage reservoirs reach their maximum limits within 20 to 25 minutes of the 30 minute rainfall event for the polygons in the middle and downstream areas. The maximum capacity for the same polygons during the 100 year return event are reached within 15 to 20 minutes. The difference when maximum capacity is reached using the two different thickness capacities is small (0 to 5 minutes).

Table 5. Time before the store reservoir under the porous asphalt reaches its full capacity (min).

	100 year return		**50 year return**		**10 year return**		**1 year return**	
	0.5 m	**0.25 m**	**0.5 m**	**0.25 m**	**0.5 m**	**0.25 m**	**0.5 m**	**0.25 m**
Polygon 1304 (upstream)	NA	NA	NA	NA	NA	NA	NA	NA
Polygon 1301 (middle part)	20 min	15 min	20 min	20 min	NA	NA	NA	NA
Polygon 1324 (downstream)	20 min	15 min	25 min	20 min	NA	NA	NA	NA

Flooding for the three top nodes for the 100 year event (no. 149, no. 153 and J5 as was shown in Figure 17) was reduced to 0 after the implementation of porous asphalt with 0.25 and 0.5 meter reservoirs. The node with the highest flooding volumes (Node 149) during the 100 year event still showed a small occurrence of flooding with the 0.25 meter reservoir thickness. Figure 22 illustrated the total flooding of the node 149 during the 100 year return rainfall event. The odd spike in during the 28-29 min of the rainfall event could be explained with the limited capacity of the Weirs routing the outpouring water from the inlets to porous asphalt. In this case the outpouring water that does not enter the channels as they have reached their maximum intake still gets classified as flooding.

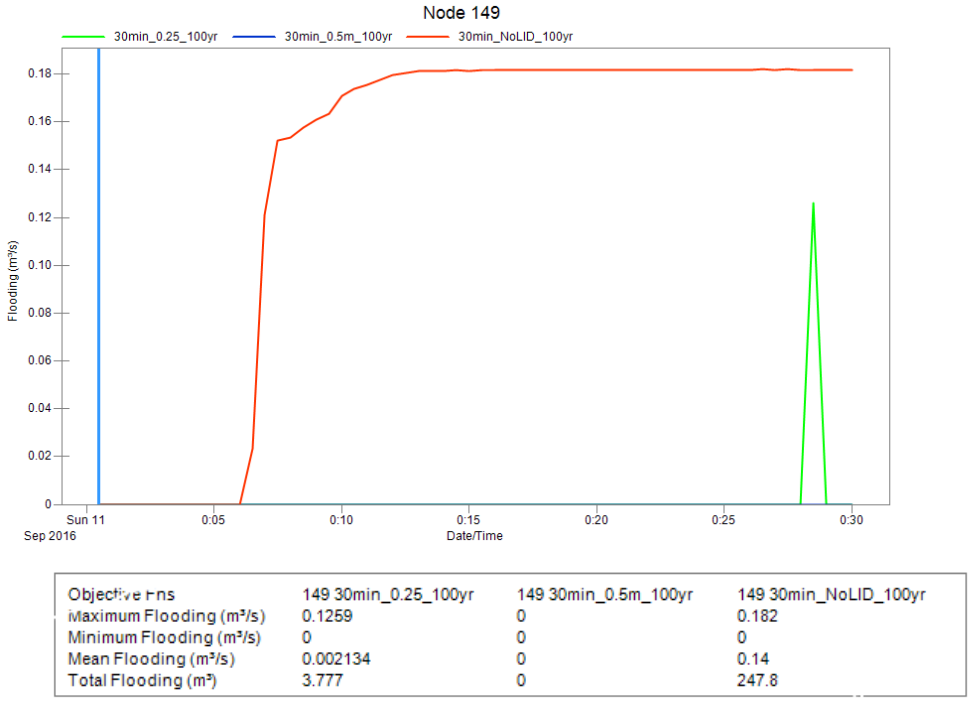

Figure 22. Flooding for Node 149 during 100 year rainfall event with 0.25 and 0.5 meter reservoirs and without porous asphalt.

The surface runoff of the polygon (Subcatchment1301) that surrounds Node 149 is changed after the implementation of porous asphalt. Without the porous pavement all of the water flowing out of Node 149 gets classified as flooding and does not get registered as runoff. In case with porous asphalt surface runoff occurs once the storage reservoir gets filled up. In case with the 0.25 meter reservoir 40.43 m^3 water gets classified as runoff and it is reduced to 18.42 m^3 during 0.5 meter reservoir for the Subcatchment 1301.

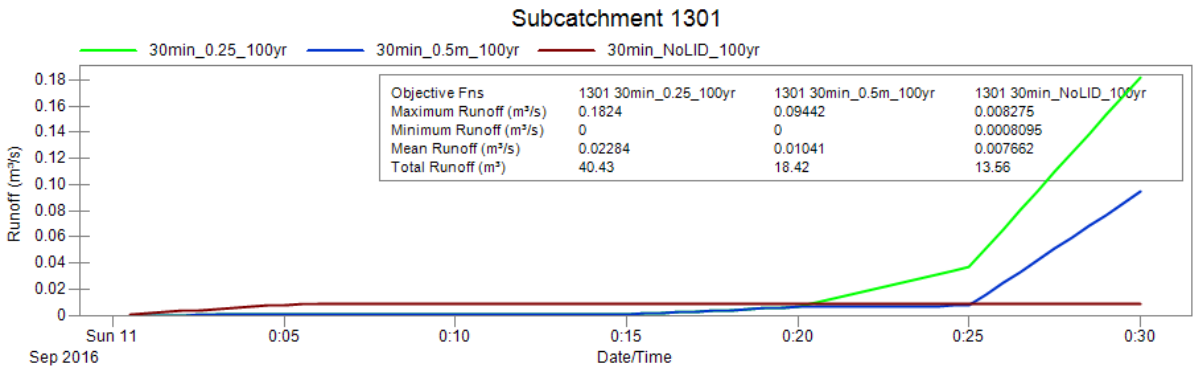

Figure 23. Surface ruoff for Subcatchment 1301 during 100 year return rainfall event.

5 Discussion

5.1 Flood reduction with varying reservoir capacities.

Porous asphalt was implemented to an area of 4370 m^2 covering the impermeable parts of Gästgivarevägen and southern parts of Vapenkroken and Källarekroken streets. With this selection the flood volume was reduced 65.6%, 77.5% and 99.2% for 100, 50 and 10 year return rainfall events respectively. No flooding was recorded with 1 year return rainfall simulations. Increasing the stone reservoir from 0.25 meters to 0.5 meters only minimally improved the total flooding volume for the whole area. The polygon specific results for the sections under porous asphalt (1304 in the upstream, 1301 in the middle part and 1324 in the downstream areas) do show that the maximum capacity of the reservoirs during the 50 and 100 year return rainfall events is reached at different times for the 0.25 meter and 0.5 meters reservoirs. The thinner reservoir gets filled up approximately 5 minutes before the thicker reservoir. This theoretically should reduce also the total flooding volume for the whole area, even though porous asphalt is not simulated across the study area, but only in the selected sections. The reason for the small overall flooded volume reduction could be due to the way PCSWMM calculates flooding amounts. As explained in Section 4.1 flooding occurs once water from the drainage pipes get pushed up from the horizontal pipes due to oncoming water and once the water reaches the same level as the rim level of the inlets this volume of water is then classified as flooding and removed from the system. In sections with porous asphalt, channel type pipes, Weirs were added to allow the water, otherwise simply classified as flooded to be routed to the surrounding porous pavement where it could infiltrate into the storage reservoir. However, once the reservoir gets filled up then the rest of the oncoming water, unless further routed to neighboring areas is simply removed from the system. It does not get classified as flooding. This can be seen from the Figure 22 that illustrates the highest flooding node (Node 149) during 100 year rainfall event where after the implementation of porous asphalt flooding in reduced to 0. However, the porous pavement that surrounds that node (Polygon 1301) has its 0.25 meter stone reservoir capacity reached after 15 minutes and 0.5 meter reservoir after 20 minutes from the start of the rainfall event. The further oncoming water does not get classified as flooding, but gets classified as surface runoff. As seen from Figure 23 surface runoff of Polygon 1301 does increase once total storage capacity has been reached. That is the reason why the total flooding volume using the two different storage

capacity designs is so similar. Flooding is only counted from inlets where the excess water is not routed to porous pavements, which is the same for both simulated reservoir cases. Inlets where the excess water is routed to porous pavements eliminates flooding as the water is either absorbed in the storage reservoir or is classified as surface runoff. However, as surface runoff is not carried on from polygon to polygon then it is difficult to estimate the effect of the accumulated water volumes that the downstream areas might be exposed to.

5.2 The design of the porous asphalt

The design of the porous asphalt was determined for its suitability in medium traffic residential area (Interpave, 2010). The general structure is shown in Figure 3 where most of the absorbed flooded water (from the surface or nearby inlets) is reintroduced to the underlying drainage system and only a small part is allowed to infiltrate to the underlying soil. This approach does not have a strong impact on reducing the total volume in the drainage system but affects the peak volumes as the stored water is allowed to enter the system with a lag. The limited infiltration into the underground also reduces the risk of destabilizing the subsoils of the surrounding areas, which could have a negative impact on the top of ground structures. For highly built up areas or with high risk of pollutant contamination an added impermeable flexible membrane lining could be added as shown in Figure 4 to stop any infiltration below the store reservoir.

The clogging factor for porous asphalt was not included in this study as discrete rainfall events with 30 minute duration were used rather than a long term rainfall simulation where the permeability of the surface layer could gradually be reduced due to the clogging effect. Although clogging problem has been proved to be a significant factor in reducing infiltration rates (Fassman and Blackbourn, 2010), well managed maintenance as suggested by Al-Rubaei et al. could still keep the porous asphalt permeability high.

5.3 The reasons of flooding in the study area

The general slope of the study area calculated based on the DEM has the direction from north-east towards south-west. The two watersheds covering the area shown in Figure 10 estimated the highest accumulated flow at the south-west corner of Vapenkroken street. Although the existing drainage system does generally follow the natural topography it does not for all of the streets. The southern parts of Vapenkroken, Källarekroken and Gästgivarevägen streets have drainage pipes flowing with the direction counter to the surface slope (south to north) and are then connected in the middle of the study area with pipes flowing towards the natural slope towards west. Flooding occurs when the capacity of the drainage system is overburdened by the amount of inflow water and causes the inlets to release the excess water. The simulation classified the excess water as flooding and reported the volume in the final status report, but did not track its movement from polygon to polygon. However, the previously recorded flood events by VA Syd in the south of the study area could be expected to be caused by the water from the overflowing inlets that would consequently flow south according to the natural topography causing the water to accumulate at the south end of the Vapenkroken street.

The failure of the drainage system could be caused by the inadequate size of the pipes that are normally not designed to cope with extreme rainfall events (such as 100 year return intensities), but also by the hampering of the flow due to sediment accumulation. Uncovering the inlets during the field work proved that sediment accumulation at the bottom of the inlet pipes could be a problem for the study area as it reduces the capacity of the system to drain the incoming stormawater.

5.4 Limitations

The study encountered two main limitations concerning the availability of input data for the modelling. First, the drainage network data received from VA Syd covered only the main pipes and manholes for the study area. Existing inlets were collected during the field work, however the measurement of invert elevation was limited due to the sediment accumulation at the bottom of the inlet pipes and bolted inlet covers. Furthermore, the way the inlets were

connected to the main drainage system had to be estimated by connecting them to the closest pipe as explained in section 3.2.6.

Secondly, due to the lack of flow measurements for the study area the model could not be validated for any specific rainfall event. Instead of using recorded rainfall for a specific day, design storm for 1, 10, 50 and 100 year return rainfall intensities based on the data by Svenskt Vatten for the Municipality of Lund were used to simulate the expected impacts on the drainage system.

6 Conclusion

This study examined how the implementation of porous asphalt with two different storage capacity designs would impact the flooding risk for a neighborhood in Lund during different rainfall intensities. The results show that after the implementation of porous asphalt with 0.25 meter storage reservoir flooding is reduced by 65.6%, 77.5% and 99.2% for the 100, 50 and 10 year return rainfall events. No flooding was recorded during the 1 year return event. Increasing the storage capacity did not further reduce flooding for the 10 and 50 year return rainfall events and only decreased it by 0.4% for the 100 year return event.

The 0.25 meter reservoir capacity to absorb stormwater runoff and flooded water from the surrounding inlets was suitable for the 1 and 10 year return rainfall events. However, the maximum capacity of the reservoirs was reached after 15 to 20 minutes after the start of the 50 and 100 year return events. The excess water that did not get absorbed into the reservoir is classified as surface runoff. However, as surface runoff of one polygon is not carried on to the downstream polygons it is difficult to estimate the effect the accumulated runoff might have on the downstream areas. Additionally, flooding in PCSWMM is only registered as the water that exceeds the rim level of the street inlets, which is then removed from the system and therefore its effect in downstream areas in not further simulated. To improve this part of the modelling surface flooding from porous asphalt sections that have reached their maximum

storing capacity should be modelled to flow to downstream areas with porous asphalt sections that have not yet reached their maximum capacity.

The study focused on the LID of porous asphalt, however as a suggestion for further research permeable pavements could be modelled together with other practices such as green roofs on top of the flat garages aligning the Gästgivarevägen street, infiltration trenches or vegetated swales at the bottom of the study area for the accumulation of the storm water.

References

Al-Rubaei, A. M., Stenglein, A. L., Viklander, M., and Blecken, G.-T., (2013) Long-Term Hydraulic Performance of Porous Asphalt Pavements in Northern Sweden Journal of Irrigation and Drainage, *Engineering* 139 (6), pp. 499-505

Ballabio, C., Panagos, P., and Monatanarella, L., (2016) Mapping topsoil physical properties at European scale using the LUCAS database. *Geoderma* 261, pp. 110–123

Bates, P. D., Horritt, M. S., and Fewtrell, T. J., (2010) A simple inertial formulation of the shallow water equations for efficient two-dimensional flood inundation modeling. *Journal of Hydrology* 387, pp. 33–45.

Beven, K. J., (2012) Rainfall-runoff modeling: the primer. 2nd ed. John Wiley & Sons, Ltd.

Butler, D. and Davies, J., (2004) Urban Drainage. 2nd ed. Spon Press

Chang, T.-J., Wanga, C.-H., and Chen, A. S., (2015) A novel approach to model dynamic flow interactions between storm sewer system and overland surface for different land covers in urban areas. *Journal of Hydrology* 524, pp. 662–679.

Dreelin, E.A., Fowler, L., and Carroll, C. R., (2006) A test of porous pavement effectiveness on clay soils during natural storm events. *Water Research*, 40 (4), pp. 799– 805.

EAPA (European Asphalt Pavement Association), (2015) Website. Accessed at [25/05/2016]: http://www.eapa.org/promo.php?c=171

EPA (Environmental Protection Agency), (2016) Website. Accessed at [11/04/2016]:

https://www.epa.gov/water-research/storm-water-management-model-swmm

Ferguson, B. K., (2005) Porous Pavements. CRC Press

Fassman, E.A. and Blackbourn, S., (2010) Urban runoff mitigation by a permeable pavement system over impermeable soils. *Journal of Hydrologic Engineering*, 15 (6), pp. 475–485.

Geels, F. W., (2006) The hygienic transition from cesspools to sewer systems (1840–1930): The dynamics of regime transformation, *Research Policy* 35 (7), pp. 1069–1082.

GSD (Geografiska Sverigedata), Lantmäteriet, (2015) Produktbeskrivning: GSD-Höjddata, grid 2+.

Han, W. S. and Burian, S. J., (2009) Determining Effective Impervious Area for Urban

Hydrologic Modeling. *Journal of Hydrologic Engineering*, 14(2), pp. 111-120.

Interpave (2010), Permeable Pavements. Ed. 6. Guide to the design, construction and maintenance of concrete block permeable pavements. Accessed at [17/04/2016]: http://www.marshalls.co.uk/dam-svc/AssetStore/Interpave-Permeable-Pavements-6434.pdf
FHWA (Federal Highway Administration), (2015) Technical Brief: Porous Asphalt Pavements with Stone Reservoirs. FHWA-HIF-15-009. Accessed at [17/04/2016]: http://www.fhwa.dot.gov/pavement/asphalt/pubs/hif15009.pdf

Janet Barco, J., Wong, K. M., and Stenstrom, M. K., (2008) Automatic Calibration of the U.S. EPA SWMM Model for a Large Urban Catchment. *Journal of Hydrologic Engineering*, 134(4), pp. 466-474.

Jain, G. V., Agrawal, R., Bhanderi, R. J., Jayaprasad, P., Patel, J. N., Agnihotri, P. G., and Samtani, B. M., (2016) Estimation of sub-catchment area parameters for Storm Water Management Model (SWMM) using geo-informatics. *Geocarto International* 31 (4), pp. 462–476.

James, W., Rossman, and James, W. R. C., (2010) User's guide to SWMM 5. 13th ed. CHI Press Publication

Jha, A. K, Bloch, R., and Lamond, J., (2012) Cities and Flooding: A Guide to Integrated Urban Flood Risk Management for the 21st Century. The World Bank, Global Facility for Disaster Reduction and Recovery. Accessed at [11/04/2016]: https://books.google.se/books?hl=en&lr=&id=n6NoKiWglh0C&oi=fnd&pg=PA6&dq=causes+of+urban+flooding&ots=izbydBQybk&sig=NitFy76EnrmZbbs01KX_9zQNJBM&redir_esc=y#v=snippet&q=cause&f=false

Kandhal, P., and Mallick, R. (1998) Open-graded friction course: State of the practice. Rep. No. E-C005, Transportation Research Board of the National Academies, Washington, DC.

Kim, H., Jung, M., Mallari, K. J. B., Pak, G., Kim, S., Kim, S., Kim, L., and Yoon, Y., (2015) Assessment of porous pavement effectiveness on runoff reduction under climate change scenarios. *Desalination and Water Treatment*, 53 (11), pp. 3142-3147.

Krebs, G., Kokkonen, T., Valtanen, M., Setälä, H., and Koivusalo, H., (2014) Spatial resolution considerations for urban hydrological modeling. *Journal of Hydrology*, 512, pp. 482–497.

Kunstmann, H., Heckl, A., and Rimmer, A., (2006) Physically based distributed hydrological modelling of the Upper Jordan catchment and investigation of effective model equations. *Advances in Geoscience*, 9, pp. 123–130.

Liu, W., Chen, W., and Peng, C. (2014) Assessing the effectiveness of green infrastructures on urban floodingreduction: A community scale study *Ecological Modelling* 291, pp. 6–14.

Lewis, D. and Purcell, P. H., (2014) *Form disaster risk reduction to resilience: a new urban agenda for the 21st century.* The United Nations Office for Disaster Risk Reduction, Global Assessment Report on disaster Risk Reduction. Accessed at [11/04/2016]: http://www.preventionweb.net/english/hyogo/gar/2015/en/bgdocs/UN-Habitat,%202014a.pdf

Länsstyrelsen Skåne, (2016) Web GIS environment. Accessed at [27/04/2016]: http://www.lansstyrelsen.se/skane/Sv/lantbruk-och-landsbygd/lantbruk/jordbruksfastigheter/Pages/jord--och-skogsklassificeringen-i-skane.aspx

Meyer S. P, Salem T. H, and Labadie J. W., (1993) Geographic information systems in urban storm-water management. *Journal of Water Resources Planning and Management*, 119, pp. 206–228.

Niea, L., Lindholma, O., Lindholmb, G., and Syversenc, E., (2009) Impacts of climate change on urban drainage systems – a case study in Fredrikstad, Norway. *Urban Water Journal* 6 (4), pp. 323–332.

Niemczynowicz, J., (1990) A detailed water budget for the city of Lund as a basis for the simulation of different future scenarios. Hydrological Processes and Water Management in Urban Areas. IAHS Publ. 198, pp. 51-58.

Palla, A., Gnecco, I., Carbone, M., Garofalo, G., Lanza, L. G., and Piro, P., (2015) Influence of stratigraphy and slope on the drainage capacity of permeable pavements: laboratory results. *Urban Water Journal*, 12 (5), pp. 394-403

Putman, B. J. and Kline, L. C. (2012) Comparison of Mix Design Methods for Porous Asphalt Mixtures Journal of Materials in Civil Engineering pp. 1359-1367.

Rodriguez, F., Andrieua, H., and Creutin, J.-D., (2003) Surface runoff in urban catchments: morphological identification of unit hydrographs from urban databanks. *Journal of Hydrology* 283, pp. 146–168

Roseen, R. M., Ballestero, T. P., Houle, J. J., Briggs, J. F., and Houle, K. M., (2012) Water Quality and Hydrologic Performance of a Porous Asphalt Pavement as a Storm-Water Treatment Strategy in a Cold Climate, *Journal of Environmental Engineering* 138 (1), pp. 81-89

Sun, N, Hong, B., and Hall, M. (2014) Assessment of the SWMM model uncertainties within the generalized likelihood uncertainty estimation (GLUE) framework for a high-resolution urban sewershed *Hydrol. Process.* 28, pp. 3018–3034.

Swedish EPA (Environmental Protection Agency), (2014) Wastewater treatment in Sweden. Accessed at [11/04/2016]: http://resolver.ebscohost.com/openurl?sid=EBSCO%3a8gh&genre=article&issn=17476585&ISBN=&volume=27&issue=2&date=20130601&spage=216&pages=216-

228&title=Water+&atitle=The+potential+to+retrofit+sustainable+drainage+systems+to+address+combined+sewer+overflow+discharges+in+the+Thames+Tideway+catchment.&aulast=Stovin%2c+Virginia+R.&id=DOI%3a10.1111%2fj.1747-6593.2012.00353.x&site=ftf-live

Swedish Water and Wastewater Association (SWWA), (2011) Nederbördsdata vid dimensionering och analys av avloppssystem. [Precipitation data for dimensioning and analysis of waste water systems]. Publication P104, Svenskt Vatten, Stockholm.

U.S. Environmental Protection Agency (EPA), (2000) Low Impact Development (LID) A Literature Review, EPA- 841-B-00-005. Accessed at [17/04/2016]: http://nepis.epa.gov/Exe/ZyPURL.cgi?Dockey=P1001B6V.txt

USDA, (2016), Natural Resources Conservation Service, Accessed at [27/04/2016]: http://www.nrcs.usda.gov/wps/portal/nrcs/detail/soils/survey/?cid=nrcs142p2_054167

VA Syd, (2012) Åtgärdsplan för Lunds avlopp (*Action Plan for Lund sewage)*

Winston, R. J., Al-Rubaei, A. M., Blecken, G. T., Viklander, M, and Hunt, W. F., (2016) Maintenance measures for preservation and recovery of permeable pavement surface infiltration rate e The effects of street sweeping, vacuum cleaning, high pressure washing, and milling. *Journal of Environmental Management*, 169, pp. 132-144

Yao, L., Wei, W, and Chen, L. (2016) How does imperviousness impact the urban rainfall-runoff processunder various storm cases? *Ecological Indicators* 60, pp.893–905.

Zhang, S., and Guo, Y. (2015) SWMM Simulation of the Storm Water Volume Control Performance of Permeable Pavement Systems. *Journal of Hydrologic Engineering*, 20 (8): 06014010

Zhang, B., Xie, G., Li, N., and Wang, S., (2015) Effect of urban green space changes on the role of rainwater runoff reduction in Beijing, China. *Landscape and Urban Planning* 140, pp. 8–16

Zahmatkesh, Z., Burian, S. J., Karamouz, M., Tavakol-Davani, H., and Goharian, E., (2015) Low-Impact Development Practices to Mitigate Climate Change Effects on Urban Stormwater Runoff: Case Study of New York City. Journal of Irrigation and Drainage Engineering 141 (1),

Appendices

Appendix 1 Filed work

Picture 1 Collecting data at Vapenkroken street

Picture 2 Collecting the coordinates of a private inlet

Picture 2 Inlet near Gästgivarevägen street

Picture 1 Uncovered inlet with accumulated sediment at the bottom

Picture 5 Bolted private inlet

Appendix 2 The Status Report

Following is the top of the status report for the 100 year return rainfall event with porous asphalt (0.25 meters)

```
****************
Analysis Options
****************
Flow Units ..............  CMS
Process Models:
  Rainfall/Runoff ........  YES
  RDII ...................  NO
  Snowmelt ...............  NO
  Groundwater ............  NO
  Flow Routing ...........  YES
  Ponding Allowed ........  NO
  Water Quality ..........  NO
Infiltration Method ......  GREEN_AMPT
Flow Routing Method ......  DYNWAVE
Starting Date ............  SEP-11-2016 00:00:00
Ending Date ..............  SEP-11-2016 00:30:00
Antecedent Dry Days ......  0.0
Report Time Step .........  00:00:30
Wet Time Step ............  00:05:00
Dry Time Step ............  01:00:00
Routing Time Step ........  5.00 sec
Variable Time Step .......  YES
Maximum Trials ...........  8
Number of Threads ........  2
Head Tolerance ...........  0.001500 m


**************************        Volume         Depth
Runoff Quantity Continuity     hectare-m            mm
**************************     ---------       -------
```

Total Precipitation	0.617	44.460
Outfall Runon	0.051	3.709
Evaporation Loss	0.000	0.000
Infiltration Loss	0.087	6.301
Surface Runoff	0.426	30.656
LID Drainage	0.000	0.021
Final Storage	0.121	8.752
Continuity Error (%)	5.064	

************************** Flow Routing Continuity **************************	Volume hectare-m ---------	Volume 10^6 ltr ---------
Dry Weather Inflow	0.000	0.000
Wet Weather Inflow	0.376	3.758
Groundwater Inflow	0.000	0.000
RDII Inflow	0.000	0.000
External Inflow	0.000	0.000
External Outflow	0.285	2.852
Flooding Loss	0.055	0.552
Evaporation Loss	0.000	0.000
Exfiltration Loss	0.000	0.000
Initial Stored Volume	0.000	0.000
Final Stored Volume	0.027	0.271
Continuity Error (%)	2.190	

Institutionen för naturgeografi och ekosystemvetenskap, Lunds Universitet.

Student examensarbete (Seminarieuppsatser). Uppsatserna finns tillgängliga på institutionens geobibliotek, Sölvegatan 12, 223 62 LUND. Serien startade 1985. Hela listan och själva uppsatserna är även tillgängliga på LUP student papers (https://lup.lub.lu.se/student-papers/search/) och via Geobiblioteket (www.geobib.lu.se)

The student thesis reports are available at the Geo-Library, Department of Physical Geography and Ecosystem Science, University of Lund, Sölvegatan 12, S-223 62 Lund, Sweden. Report series started 1985. The complete list and electronic versions are also electronic available at the LUP student papers (https://lup.lub.lu.se/student-papers/search/) and through the Geo-library (www.geobib.lu.se)

372 Andreas Dahlbom (2016) The impact of permafrost degradation on methane fluxes - a field study in Abisko

373 Hanna Modin (2016) Higher temperatures increase nutrient availability in the High Arctic, causing elevated competitive pressure and a decline in *Papaver radicatum*

374 Elsa Lindevall (2016) Assessment of the relationship between the Photochemical Reflectance Index and Light Use Efficiency: A study of its seasonal and diurnal variation in a sub-arctic birch forest, Abisko, Sweden

375 Henrik Hagelin and Matthieu Cluzel (2016) Applying FARSITE and Prometheus on the Västmanland Fire, Sweden (2014): Fire Growth Simulation as a Measure Against Forest Fire Spread – A Model Suitability Study –

376 Pontus Cederholm (2016) Californian Drought: The Processes and Factors Controlling the 2011-2016 Drought and Winter Precipitation in California

377 Johannes Loer (2016) Modelling nitrogen balance in two Southern Swedish spruce plantations

378 Hanna Angel (2016) Water and carbon footprints of mining and producing Cu, Mg and Zn: A comparative study of primary and secondary sources

379 Gusten Brodin (2016) Organic farming's role in adaptation to and mitigation of climate change - an overview of ecological resilience and a model case study

380 Veränika Trollblad (2016) Odling av *Cucumis Sativus* L. med aska från träd som näringstillägg i ett urinbaserat hydroponiskt system

381 Susanne De Bourg (2016) Tillväxteffekter för andra generationens granskog efter tidigare genomförd kalkning

382 Katarina Crafoord (2016) Placering av energiskog i Sverige - en GIS analys

383 Simon Nåfält (2016) Assessing avalanche risk by terrain analysis An experimental GIS-approach to The Avalanche Terrain Exposure Scale (ATES)

384 Vide Hellgren (2016) Asteroid Mining - A Review of Methods and Aspects

385 Tina Truedsson (2016) Hur påverkar snömängd och vindförhållande vattentrycksmätningar vintertid i en sjö på västra Grönland?

386 Chloe Näslund (2016) Prompt Pediatric Care Pediatric patients' estimated travel times to surgically-equipped hospitals in Sweden's Scania County

387 Yufei Wei (2016) Developing a web-based system to visualize vegetation trends

by a nonlinear regression algorithm

388 Greta Wistrand (2016) Investigating the potential of object-based image analysis to identify tree avenues in high resolution aerial imagery and lidar data

389 Jessica Ahlgren (2016) Development of a Web Mapping Application for grazing resource information in Kordofan, Sudan, by downloading MODIS data automatically via Python

390 Hanna Axén (2016) Methane flux measurements with low-cost solid state sensors in Kobbefjord, West Greenland

391 Ludvig Forslund (2016) Development of methods for flood analysis and response in a Web-GIS for disaster management

392 Shuzhi Dong (2016) Comparisons between different multi-criteria decision analysis techniques for disease susceptibility mapping

393 Thirze Hermans (2016) Modelling grain surplus/deficit in Cameroon for 2030

394 Stefanos Georganos (2016) Exploring the spatial relationship between NDVI and rainfall in the semi-arid Sahel using geographically weighted regression

395 Julia Kelly (2016) Physiological responses to drought in healthy and stressed trees: a comparison of four species in Oregon, USA

396 Antonín Kusbach (2016) Analysis of Arctic peak-season carbon flux estimations based on four MODIS vegetation products

397 Luana Andreea Simion (2016) Conservation assessments of Văcărești urban wetland in Bucharest (Romania): Land cover and climate changes from 2000 to 2015

398 Elsa Nordén (2016) Comparison between three landscape analysis tools to aid conservation efforts

399 Tudor Buhalău (2016) Detecting clear-cut deforestation using Landsat data: A time series analysis of remote sensing data in Covasna County, Romania between 2005 and 2015

400 Sofia Sjögren (2016) Effective methods for prediction and visualization of contaminated soil volumes in 3D with GIS

401 Jayan Wijesingha (2016) Geometric quality assessment of multi-rotor unmanned aerial vehicle-borne remote sensing products for precision agriculture

402 Jenny Ahlstrand (2016) Effects of altered precipitation regimes on bryophyte carbon dynamics in a Peruvian tropical montane cloud forest

403 Peter Markus (2016) Design and development of a prototype mobile geographical information system for real-time collection and storage of traffic accident data

404 Christos Bountzouklis (2016) Monitoring of Santorini (Greece) volcano during post-unrest period (2014-2016) with interferometric time series of Sentinel-1A

405 Gea Hallen (2016) Porous asphalt as a method for reducing urban storm water runoff in Lund, Sweden

406 Marcus Rudolf (2016) Spatiotemporal reconstructions of black carbon, organic matter and heavy metals in coastal records of south-west Sweden

407 Sophie Rudbäck (2016) The spatial growth pattern and directional properties of *Dryas octopetala* on Spitsbergen, Svalbard